THE JOURNAL OF PHYSICAL CHEMISTRY B

Article

pubs.acs.org/JPCB

Na/Ca Intermixing around Silicate and Phosphate Groups in Bioactive Phosphosilicate Glasses Revealed by Heteronuclear Solid-State NMR and Molecular Dynamics Simulations

Renny Mathew, Baltzar Stevensson, and Mattias Edén*

Physical Chemistry Division, Department of Materials and Environmental Chemistry, Arrhenius Laboratory, Stockholm University, SE-106 91 Stockholm, Sweden

Supporting Information

ABSTRACT: We characterize the intermixing of network-modifying Na^+/Ca^{2+} ions around the silicate (Q^n_{Si}) and phosphate (Q^n_P) tetrahedra in a series of 16 $Na_2O-CaO-SiO_2-P_2O_5$ glasses, whose P content and silicate network connectivity were varied independently. The set includes both bioactive and bio*in*active compositions and also encompasses two soda-lime-silicate members devoid of P, as well as two $CaO-SiO_2$ glasses and one $Na_2O-SiO_2-P_2O_5$ glass. The various Si/P↔Na/Ca contacts were probed by molecular dynamics (MD) simulations together with heteronuclear magic-angle-spinning (MAS) nuclear magnetic resonance (NMR) experimentation utilizing $^{23}Na\{^{31}P\}$ and $^{23}Na\{^{29}Si\}$ REDOR, as well as $^{31}P\{^{23}Na\}$ and $^{29}Si\{^{23}Na\}$ REAPDOR. We introduce an approach for quantifying the extent of Na^+/Ca^{2+} ordering around a given Q^n_P or Q^n_{Si} group, encoded by the preference factor $0 \leqslant P_M \leqslant 1$ conveying the relative weights of a random cation intermixing ($P_M = 0$) and complete preference/ordering ($P_M = 1$) for one of the species M, which represents either Na^+ or Ca^{2+}. The MD-derived preference factors reveal phosphate and silicate species surrounded by Na^+/Ca^{2+} ions intermixed nearly randomly ($P_M \lesssim 0.15$), except for the Q^4_{Si} and Q^1_{Si} groups, which manifest more significant cation ordering with preference for Na^+ and Ca^{2+}, respectively. The overall weak preferences are essentially independent of the Si and P contents of the glass, whereas P_M primarily correlates with the total amount of network modifiers: as the latter is increased, the Na/Ca distribution around the $\{Q^0_P, Q^1_{Si}, Q^2_{Si}\}$ groups with preference for Ca^{2+} tend to randomize (i.e., P_{Ca} decreases), while the P_{Na}-values grow slightly for the $\{Q^1_P, Q^3_{Si}, Q^4_{Si}\}$ species already preferring coordination of Na. The set of experimental preference factors $\{P_{Ca}\}$ for the orthophosphate (Q^0_P) groups extracted from $^{31}P\{^{23}Na\}$ REAPDOR NMR-derived M_2(P−Na) dipolar second moments agrees well with the MD-generated counterparts. Our results on the Na/Ca intermixing in soda-lime-silicate glasses are discussed in relation to previous reports, highlighting the dependence of the conclusion on the approach to data evaluation.

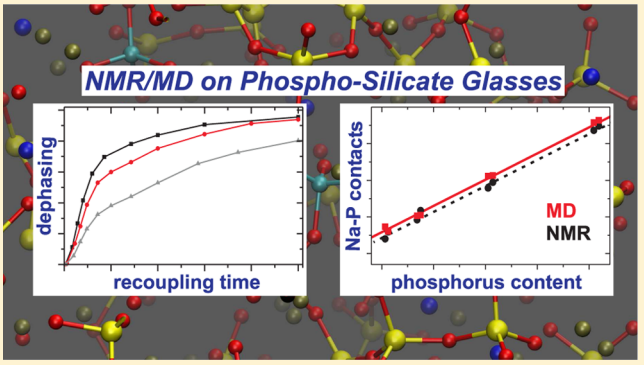

1. INTRODUCTION

Although the archetypal random glass network model of Zachariasen[1] is doubtlessly oversimplified, it is often unclear what extent of deviations the "real" (modified) silicate glass structure manifests.[2,3] The distribution of network-modifying cations in multicomponent glasses affect their physical properties and is believed to be the key to understand anomalies such as the "mixed alkali effect".[4−7] Considering the intermixing of M_1^+/M_2^+ (alkali/alkali) and M_1^+/M_2^{2+} (alkali/alkaline-earth) cations among themselves or around network-forming groups, many studies are reported on ternary glass systems based on a sole glass network former, e.g., B_2O_3, P_2O_5 or SiO_2,[2,5,7−14] including soda-lime-silicate glasses.[15−19]

However, the relative preferences for silicate/phosphate associations with Na/Ca in $Na_2O-CaO-SiO_2-P_2O_5$ glasses are very sparsely explored experimentally.[20] Some of these glasses are *bioactive*, meaning that they bond to bone/tooth via a biomimetic surface layer of hydroxy-carbonate apatite (HCA) forming when the glass is exposed to body fluids.[21] A phosphosilicate glass involves a network of interconnected SiO_4 tetrahedra; Q^n_{Si} denotes one such group with n bridging oxygen (BO) atoms and 4−n nonbridging oxygen (NBO) ions.[3] The P speciation is dominated by orthophosphate (Q^0_P) groups, with minor contributions from Q^1_P moieties[3,22−32] that involve one P−O−Si bridge.[25−29,31−33] Knowledge of the relative propensities for Na and Ca to associate with the various Q^n_T (T = {Si, P}) groups may assist rationalization of composition−solubility/bioactivity relationships of bioactive glasses (BGs).

Received: February 3, 2015
Revised: March 25, 2015
Published: March 27, 2015

DOI: 10.1021/acs.jpcb.5b01130
J. Phys. Chem. B 2015, 119, 5701−5715

Table 1. Glass Compositions[a]

label	$\overline{N}^{Si}_{BO}$(nom)[b]	aNa_2O	$bCaO$	$cSiO_2$	dP_2O_5	ρ_{BG} (g cm^{-3})[c]	$\rho(M_{tot})$ (nm^{-3})[c]	ρ_{Na} (nm^{-3})[c]	ρ_{Ca} (nm^{-3})[c]	ρ_{Si} (nm^{-3})[c]	ρ_P (nm^{-3})[c]
BG^{0}_{0}(2.0)	2.00	0.000(−)	0.500(0.491)	0.500(0.509)	0.000(−)	2.894	15.00	−	15.00	15.00	−
$BG^{0.48}_{2.6}$(2.1)	2.11	0.244(0.229)	0.269(0.255)	0.461(0.486)	0.026(0.030)	2.704	19.96	12.86	7.11	12.21	1.38
$BG^{0.41}_{6.0}$(2.1)	2.15	0.221(0.207)	0.324(0.315)	0.395(0.412)	0.060(0.065)	2.743	19.74	11.39	8.36	10.17	3.09
BG^{0}_{0}(2.5)	2.50	0.000(−)	0.428(0.412)	0.572(0.588)	0.000(−)	2.817	12.44	−	12.44	16.63	−
$BG^{0.43}_{0}$(2.5)	2.50	0.186(0.178)	0.242(0.231)	0.572(0.591)	0.000(−)	2.673	16.62	10.07	6.55	15.48	−
$BG^{0.43}_{1.0}$(2.5)	2.50	0.192(0.181)	0.249(0.250)	0.549(0.559)	0.010(0.010)	2.685	16.97	10.28	6.69	14.73	0.54
$BG^{0.43}_{2.0}$(2.5)	2.50	0.197(0.191)	0.257(0.258)	0.526(0.527)	0.020(0.024)	2.691	17.26	10.47	6.79	13.95	1.04
$BG^{0.43}_{4.0}$(2.5)	2.50	0.209(0.193)	0.271(0.254)	0.480(0.509)	0.040(0.044)	2.693	17.77	10.77	7.00	12.43	2.10
$BG^{0.43}_{6.0}$(2.5)	2.50	0.219(0.201)	0.287(0.274)	0.434(0.460)	0.060(0.065)	2.707	18.38	11.16	7.22	11.00	3.08
$BG^{1.00}_{6.0}$(2.5)	2.50	0.506(n.a.)	0.000(n.a.)	0.434(n.a.)	0.060(n.a.)	2.569	23.68	23.68	−	10.17	2.85
$BG^{0.48}_{2.6}$(2.7)	2.74	0.202(0.194)	0.222(0.214)	0.550(0.560)	0.026(0.032)	2.640	16.09	10.38	5.71	14.15	1.33
$BG^{0.43}_{0}$(2.9)	2.93	0.151(0.143)	0.197(0.183)	0.652(0.674)	0.000(−)	2.600	13.11	7.94	5.18	17.14	−
$BG^{0.43}_{2.0}$(2.9)	2.93	0.165(0.151)	0.215(0.206)	0.600(0.623)	0.020(0.020)	2.624	14.02	8.47	5.55	15.48	1.07
$BG^{0.43}_{3.0}$(2.9)	2.93	0.172(0.161)	0.224(0.226)	0.574(0.583)	0.030(0.030)	2.625	14.49	8.77	5.72	14.64	1.53
$BG^{0.43}_{4.0}$(2.9)	2.93	0.179(0.162)	0.233(0.226)	0.548(0.572)	0.040(0.040)	2.639	14.93	9.03	5.91	13.86	2.05
$BG^{0.43}_{6.0}$(2.9)	2.93	0.193(0.172)	0.252(0.244)	0.495(0.524)	0.060(0.060)	2.661	15.88	9.63	6.25	12.36	2.98

[a]The $BG^{q}_{p}(\overline{N}^{Si}_{BO})$ glasses are grouped according to increasing silicate network connectivity ($\overline{N}^{Si}_{BO}$) and P_2O_5 content (p mol % P_2O_5). q represents the molar fraction $q = n(Na_2O)/[n(Na_2O) + n(CaO)]$. The coefficients $\{a, b, c, d\}$ specify the *nominally* batched aNa_2O−$bCaO$−$cSiO_2$−dP_2O_5 oxide equivalents with $a + b + c + d = 1$; values within parentheses are compositions obtained by SEM/EDS. [b]$\overline{N}^{Si}_{BO}$(nom) corresponds to the *nominal* value of the network connectivity (see ref 32). [c]ρ_{BG} represents the glass density (uncertainty ±0.003 gcm^{-3}), determined by the Archimedes method in water at 25 °C. ρ_E denotes the *number density* of element E, $\rho_E = n_E N_A/V_m$ (N_A and V_m is Avogadro's number and the molar volume, respectively), as estimated from ρ_{BG} and the *nominal* glass composition; $\rho(M_{tot}) = \rho_{Na}+\rho_{Ca}$.

Given the limited number of experimental studies informing *directly* about *medium*-range (0.3−1 nm) structural features of P-bearing soda-lime-silicate glasses,[20,31,33−35] the most detailed insight stems from molecular dynamics (MD) simulations, where several structural inhomogeneities have been suggested,[20,25,26,29] e.g., "phosphate clustering" and strong Ca−P affinities (relative to Na−P) leading to Na-depleted calcium phosphate aggregates in BGs that are rich in either Si or P.[25,26,29] Such phosphate aggregation together with significant ring formation of interconnected SiO_4 groups are suggested as nanoscale features inhibiting glass degradation in aqueous media and thereby reducing the bioactivity.[25,26,29] In contrast, ^{31}P NMR chemical shifts from Na−Ca−Si−P−O glasses suggest mixed Na/Ca environments around the orthophosphate groups:[20,22−24,26,32,34,36] a continuous ^{31}P magic-angle-spinning (MAS) NMR peak-displacement observed when the modifier content of the glass is varied indicates an essentially statistical Na^+/Ca^{2+} partitioning around the Q^0_P moieties.[22,23,32,36] The corresponding trends of the Na/Ca−SiO_4 contacts are less explored.[17,22−24,30,32] Unfortunately, the information from *short*-range ^{31}P, ^{29}Si, or ^{23}Na chemical shift interactions is only *indirect*. Yet, ^{17}O NMR offers a richer information source, owing to its sensitivity to different network modifier-constellations around the BO/NBO species.[9,13,15,20] It has hitherto only been applied to one phosphosilicate composition (the "45S5 Bioglass"[21]), revealing a dominance of mixed Na/Ca−PO_4 and Na/Ca−SiO_4 environments, with a *depletion* of Ca−PO_4 contacts relative to a strictly statistical Na/Ca intermixing,[20] in stark contrast to predictions from MD simulations.[25,26,29]

However, all experimental and computational studies of Na_2O−CaO−SiO_2−P_2O_5 glasses to date have focused on a small number of glass compositions that are insufficient for establishing and rationalizing potential trends of the nature of the Ca/Na−Si/P associations when the BG composition varies. Furthermore, no transparent *quantification* of the *extents* of cation ordering is reported. Hence, herein we seek to rationalize the apparently discrepant inferences made from MD simulations and various NMR studies by applying both techniques to a large series of Na−Ca−Si−P−O glasses with variable compositions. We introduce alternative assessment strategies of the MD-modeled data (compared to those previously adopted[20,25,26,29,37]) in conjunction with ^{23}Na and ^{31}P MAS NMR, as well as heteronuclear dipolar recoupling MAS NMR techniques that are sensitive to the Na−P and Na−Si through-space contacts[2,12,14,38−41] (applied here for the first time to probe the Na/Ca intermixing in phosphosilicate glasses); this allows us to (*i*) clarify how the Na^+/Ca^{2+} cations preferentially distribute around the various Q^n_T groups in the glass structure; (*ii*) *quantify* these preferences relative to each limiting scenario of a statistical distribution and a complete clustering/segregation of one species alone around Q^n_T, and (*iii*) identify the primary composition-dependencies of the relative (Ca/Na)↔(Si/P) contacts.

2. PHOSPHOSILICATE GLASS SAMPLES

Table 1 lists the 16 soda-lime-silica based glasses considered herein, each labeled $BG^{q}_{p}(\overline{N}^{Si}_{BO})$, where p is the P_2O_5 content in mol %, $q = n(Na_2O)/[n(Na_2O)+n(CaO)]$ denotes the molar fraction of Na_2O out of the total glass modifier content, and $\overline{N}^{Si}_{BO}$ is the *silicate* network connectivity, i.e., the average number of BO atoms per SiO_4 tetrahedron.[32,42−44] Throughout, n_E or $n(E)$ denotes the stoichiometric amount of species E, whereas ρ_E is the corresponding number density. Other structural

DOI: 10.1021/acs.jpcb.5b01130
J. Phys. Chem. B 2015, 119, 5701−5715

aspects of the *mixed* Na/Ca glasses were analyzed in our previous work,[32,33] which reported the $^{29}Si/^{31}P$ NMR spectra and MD/NMR-derived fractional populations of the Q^n_{Si} and Q^n_P species (denoted $\{x^n_{Si}\}$ and $\{x^n_P\}$, respectively),[32] as well as characterization of the spatial distribution of phosphate groups.[33] Herein, we elucidate the relative glass former/modifier contacts in this glass series, which has been expanded to encompass one $Na_2O-SiO_2-P_2O_5$ $[BG^{1.00}_{6.0}(2.5)]$ and two $CaO-SiO_2$ $[BG^0_0(2.0), BG^0_0(2.5)]$ specimens.

The $BG^q_p(\overline{N}^{Si}_{BO})$ glass-set spans the compositional range 15−51 mol % Na_2O, 20−50 mol % CaO, and 40−65 mol % SiO_2, sampling the parameter space $2.0 \leqslant \overline{N}^{Si}_{BO} \leqslant 2.9$, $p \leqslant 6.0$ mol %, and $q = \{0.41, 0.43, 0.48\}$; see Table 1. Each $\{p, q, \overline{N}^{Si}_{BO}\}$ parameter independently affects the bioactivity of the glass,[32,42−45] which is our primary reason for introducing a new $Na_2O-CaO-SiO_2-P_2O_5$ glass parametrization; see Mathew et al.[32] for details. For instance, $BG^{0.48}_{2.6}(2.1)$ denotes the "45S5" composition of Hench.[21] Inherent to our glass design is that the total modifier content is selected to allow for full charge compensation of P as orthophosphate groups and simultaneously arrange an arbitrary $\overline{N}^{Si}_{BO}$ value. Consequently, the *total* modifier number density $\rho(M_{tot}) = \rho_{Na} + \rho_{Ca}$ in the glass grows concomitantly with ρ_P but decreases as $\overline{N}^{Si}_{BO}$ is increased.[32,36]

3. HETERONUCLEAR DOUBLE-RESONANCE NMR EXPERIMENTATION

Medium-range structural features in glasses—such as the spatial arrangement of N_I nuclei of species I (with spin quantum number I) around a central nucleus S of another type (with quantum number S)—may be assessed by exploiting the N_I S−I_k through-space-mediated heteronuclear dipolar interactions of the SI_{N_I} cluster (k = 1, 2, ..., N_I).[2,3] One such S−I pair is characterized by the *dipolar coupling constant* b_{S-I} (in units of s^{-1} = Hz), relating to the internuclear distance r_{S-I} according to $b_{S-I} = -\mu_0\hbar\gamma_S\gamma_I/(8\pi^2 r^3_{S-I})$, where γ_S and γ_I denote the magnetogyric ratios of the spin species S and I, respectively. Note that a *short* S−I_k interatomic distance is associated with a *large* dipolar coupling constant. However, a glass features a large number of distinct $S_jI_{N_I}$ aggregates (j = 1, 2, ..., N_S) that yields a distribution of heteronuclear r^{jk}_{S-I} distances and corresponding b^{jk}_{S-I} dipolar coupling constants. Although it is not possible to determine the individual dipolar interactions, the van Vleck *dipolar second moment*[46] is experimentally accessible:

$$M_2(\mathrm{S-I}) = \frac{4I(I+1)}{15N_S}\sum_j^{N_S}\sum_k^{N_I}(b^{jk}_{S-I})^2 = \frac{\mu_0^2\hbar^2\gamma_S^2\gamma_I^2 I(I+1)}{240\pi^4 N_S}\sum_j^{N_S}\sum_k^{N_I}(r^{jk}_{S-I})^{-6}\ [\text{unit: } s^{-2} = Hz^2] \quad (1)$$

Our usage of the term "S−I *contact*" reflects M_2(S−I), as it accounts for *both* the number N_I of I-spins around the central S-spin site j, as well as the set of distances $\{r^{jk}_{S-I}\}$.

The M_2(S−I)-value may be determined experimentally by S{I} heteronuclear MAS NMR techniques.[2,38−41,47] The S-spin NMR signal is then detected after a temporary recoupling of the MAS-averaged S−I dipolar interaction during an even integer number of rotational periods τ_r: $\tau_{rec} = 2n\tau_r$, where $\tau_r = \nu_r^{-1}$ and ν_r is the MAS frequency in units of Hz. Such a *dipolar dephasing* experiment yields an attenuated S-spin signal $[S(\tau_{rec})]$ relative to that observed in the absence of S−I recoupling, $S_0(\tau_{rec})$. The normalized signal $\Delta S/S_0 = [S_0(\tau_{rec}) - S(\tau_{rec})]/S_0(\tau_{rec})$ is proportional to the heteronuclear S−I dipolar second moment M_2(S−I):[2,40,41,47]

$$\Delta S/S_0 = \frac{4A}{I(I+1)}M_2(\mathrm{S-I})\tau^2_{rec}\{1 - [B\cdot M_2(\mathrm{S-I})\tau^2_{rec}] + \cdots\} \quad (2)$$

Hence, for *short* recoupling intervals obeying $M_2(\mathrm{S-I})\tau^2_{rec} \ll 1$, the NMR signal-dephasing depends parabolically on τ_{rec}, whereas $\Delta S/S_0$ approaches unity for large τ_{rec}-values because $S(\tau_{rec}) \approx 0$. The constants A and B are given in ref 47.

The precise heteronuclear recoupling implementations used herein are depicted in Figure **S1** of the Supporting Information (SI). $^{23}Na\{^{31}P\}$ and $^{23}Na\{^{29}Si\}$ REDOR[38] NMR were employed to estimate the respective M_2(Na−P) and M_2(Na−Si) values of the $BG^q_p(\overline{N}^{Si}_{BO})$ structures. REDOR reintroduces the S−I through-space interactions by a series of rotor-synchronized 180° pulses applied to the I spins, while the reference experiment leading to $S_0(\tau_{rec})$ utilizes a Hahn spin−echo with a total delay of $2n\tau_r$. The dipolar second moments M_2(P−Na) and M_2(Si−Na), on the other hand, were estimated via $^{31}P\{^{23}Na\}$ and $^{29}Si\{^{23}Na\}$ REAPDOR NMR experiments.[2,39] Here the 180° recoupling pulses are applied to the detected S-spins (S = 1/2), whereas an adiabatic-passage pulse is applied to ^{23}Na (i.e., the I-spins) at the center of the recoupling interval ($\tau_{rec}/2$); the latter pulse is omitted in the $[S_0(\tau_{rec})]$ reference experiment.[2,39]

4. MATERIALS AND METHODS

4.1. Glass Preparation and Characterization. The glasses were prepared with a standard melt−quench procedure in an electric furnace, using ball-milled mixtures of NaH_2PO_4 (99.99%; Merck), and Na_2CO_3 (99.9%), $CaCO_3$ (99.9%), and SiO_2 (99.99%) from ChemPur, including paramagnetic doping by 0.1 wt % Fe_2O_3. Each batch of 6.0 g was first heated in a Pt crucible at 950 °C for 4 h to ensure complete carbonate removal, whereupon the temperature was raised to 1350−1620 °C (depending on the glass composition) and held for 4 h. The melt was quenched by immersing the bottom of the crucible in water. Two additional specimens of the $BG^{0.43}_{6.0}(2.5)$ and $BG^{1.00}_{6.0}(2.5)$ compositions were prepared in 0.35 g batches from $^{29}SiO_2$ (99.9% ^{29}Si; EUROISO-TOP, France) as a precursor under otherwise identical preparation conditions but without Fe^{3+} doping.

Scanning electron microscopy (SEM) in backscatter mode verified that each sample constituted a single homogeneous amorphous phase (except for a minor inhomogeneity of the $BG^{0.43}_{6.0}(2.9)$ specimen[32,33]), while powder X-ray diffraction evidenced the absence of crystalline impurities. SEM coupled with energy-dispersive X-ray spectroscopy (EDS) revealed a good agreement between the nominally batched and the EDS-analyzed glass compositions, with the deviations remaining within the uncertainty of the measurements (see Table 1).

4.2. MD Simulations. Classical atomistic MD simulations utilizing a polarizable shell-model potential were performed with the DLPOLY3 program[48,49] for NVT ensembles of {Na, Ca, Si, P, O} atoms placed in a cubic box with periodic boundary conditions to match the *nominal* element composition and the experimental glass density (Table 1). Each melt−quench protocol started from a random atom configuration that was pre-equilibrated for 100 ps at 3500 K, followed by a 10 K/ps cooling down to 300 K in steps of 10 ps. The ensemble was then "equilibrated" for 200 ps, with 7500 samples of the last

DOI: 10.1021/acs.jpcb.5b01130
J. Phys. Chem. B 2015, 119, 5701−5715

150 ps averaged to yield the structural data. For each glass composition, this procedure was completed 2−4 times for different initial atom configurations, from which the average value and uncertainty of each structural parameter was derived. By exploiting the periodic boundary conditions, fully converged dipolar second moments were calculated from eq 1. The coordination number $Z(\alpha-\beta)$ [or $Z_{\alpha-\beta}$] of species β around α was calculated either by integrating the partial pair distribution function (PDF) $g_{\alpha-\beta}(r)$ out to its first minimum (unless a given cutoff radius is specified) or by requiring shared O species *via* $T-O-M$ bridges, where T = {Si, P} and M = {Na, Ca}. The SI provides additional computational details.

4.3. Solid-State NMR. The NMR experimentation was performed with Bruker Avance-III spectrometers at magnetic fields (B_0) of either 9.4 T or 14.1 T that correspond to Larmor frequencies of −400.07 MHz and −600.12 MHz for ^{1}H, respectively. The heteronuclear NMR experimentation is described in detail in the SI. ^{29}Si and ^{31}P MAS NMR spectra were recorded at 9.4 T with 7 mm zirconia rotors spinning at 7.00 kHz and 90° pulses operating at nutation frequencies ν_1^{Si} = 54 kHz (^{29}Si) or ν_1^{P} = 60 kHz (^{31}P). Relaxation delays of 100−150 s (^{29}Si) and 80−100 s (^{31}P) were employed for all Fe^{3+}-doped samples to ensure quantitative results. The corresponding NMR spectra of the ^{29}Si-enriched (and undoped) glass samples were recorded with a 4 mm MAS probehead under the following conditions: ν_r = 10.00 kHz, ν_1^{P} = 80 kHz, and 900 s relaxation delays for ^{31}P; ν_r = 14.00 kHz, ν_1^{Si} = 60 kHz, and 2000 s relaxation delays for ^{29}Si. The ^{23}Na MAS NMR spectra were obtained at 14.1 T, using 3.2 mm rotors spinning at 24.00 kHz. The NMR acquisitions utilized short rf pulses (0.5 μs) at ν_1^{Na} = 83 kHz. The spectral window and relaxation delays were 400 kHz and 2 s, respectively. ^{23}Na nutation frequencies were calibrated with a 0.1 M NaCl(aq) solution. ^{23}Na, ^{29}Si, and ^{31}P (chemical) shifts are reported relative to 0.1 M NaCl(aq), neat tetramethylsilane, and 85% H_3PO_4, respectively.

5. RESULTS AND DISCUSSION

5.1. Local ^{31}P and ^{23}Na Environments. Before examining the relative (Na/Ca)↔(Si/P) contacts conveyed *directly* by MD simulations and heteronuclear NMR experimentation, we inspect the *indirect* information provided from the *short*-range ^{31}P and ^{23}Na chemical shift interactions.

5.1.1. ^{31}P MAS NMR. Figure 1a shows representative ^{31}P MAS NMR spectra of the $Na_2O-CaO-SiO_2-P_2O_5$ glasses. They reflect a dominance of Q_P^0 groups that constitutes 80−96% of all phosphate species in the mixed Ca/Na BGs (see Table S1 and ref 32), with the remaining represented by Q_P^1 moieties that are responsible for the "tail" appearing at lower shifts of each ^{31}P NMR peakshape, as discussed in previous work.[22−24,27,28,30−32] The peak-maximum position of the ^{31}P resonance depends primarily on the average numbers of Na^+/Ca^{2+} cations charge-balancing the Q_P^n groups, whereas the full width at half-maximum (fwhm) of the ^{31}P NMR signal reflects the *distribution* of isotropic ^{31}P chemical shifts stemming from a spread of distinct (Na^+, Ca^{2+}) constellations around the Q_P^0 units in the glass structure. Note that Figure 1a reveals a distinctly different ^{31}P NMR spectrum from the Ca-free $BG_{6.0}^{1.00}(2.5)$ structure relative to its Ca-bearing counterpart $BG_{6.0}^{0.43}(2.5)$. The NMR peak from $BG_{6.0}^{1.00}(2.5)$ is centered at a higher chemical shift (implying less shielded ^{31}P nuclei), while the fwhm of the NMR signal only amounts to 2.6 ppm. The markedly reduced chemical-shift distribution observed from $BG_{6.0}^{1.00}(2.5)$ reflects more ordered local ^{31}P environments in the

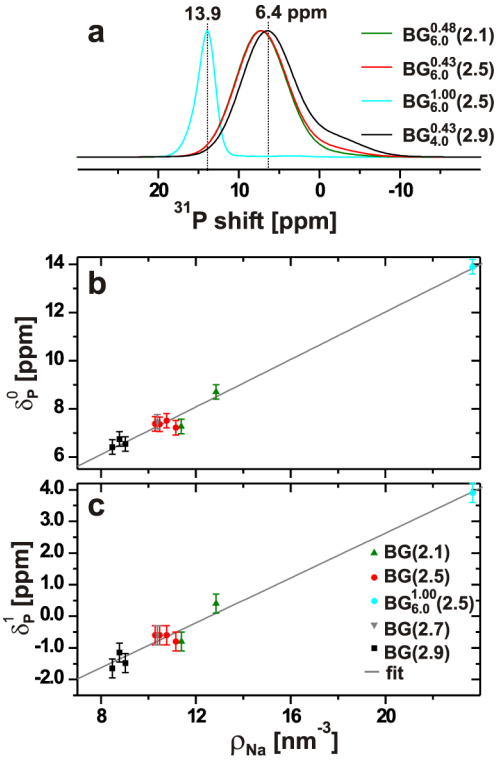

Figure 1. (a) Selection of ^{31}P MAS NMR spectra recorded from $Na_2O-(CaO)-SiO_2-P_2O_5$ glasses that feature a high P_2O_5 content and variable silicate network connectivities. (b, c) Average ^{31}P chemical shifts of (b) Q_P^0 and (c) Q_P^1 moieties, plotted against the number density of Na^+ in the glass. Each symbol and color distinguishes the data from $BG(\overline{N}_{BO}^{Si})$ branches featuring a fixed $\overline{N}_{BO}^{Si}$-value. The straight lines constitute best-fit results.

structure because only Na^+ ions charge-compensate its PO_4 moieties, in contrast to those of the Na−Ca−Si−P−O glasses.[22] Moreover, the Q_P^1 population (x_P^1 = 0.03) in $BG_{6.0}^{1.00}(2.5)$ is significantly lower than those of the Ca-bearing glasses with $\overline{N}_{BO}^{Si}$ = 2.5; $x_P^1 \approx 0.1$ (see Table S1).

The presence of *variable* (Na^+, Ca^{2+}) mixed-cation constellations around all phosphate species in the $Na_2O-CaO-SiO_2-P_2O_5$ glasses is witnessed by Figure 1(b, c), which plot the average chemical shifts of the Q_P^0 and Q_P^1 groups against the number density of Na^+ (ρ_{Na}) in each glass. Within the uncertainties of the NMR spectra deconvolutions (see Mathew et al.[32]), the chemical shift for each Q_P^n type depends roughly linearly on ρ_{Na} and tend toward lower values as $\overline{N}_{BO}^{Si}$ is increased. Throughout all Na−Ca−Si−P−O glasses, the fwhm of the ^{31}P NMR signals from the Q_P^0 and Q_P^1 groups remain fairly constant ≈7.5 ppm and 8−9 ppm, respectively.

5.1.2. ^{23}Na MAS NMR. Figure 2(a, b) display a selection of ^{23}Na NMR spectra from BGs featuring either increasing $\overline{N}_{BO}^{Si}$-values [and thereby increasing $\rho(M_{tot})$] at (a) a nearly constant P_2O_5 content of 2−3 mol %, or (b) growing P_2O_5 contents at fixed $\overline{N}_{BO}^{Si}$ = 2.50. Although the quadrupolar nature of ^{23}Na may give significant broadening from second-order quadrupolar interactions,[2,3] the nearly Gaussian NMR peakshapes obtained at the relatively high external magnetic field of B_0 = 14.1 T suggest that chemical-shift distributions mainly account for the observed resonance-broadening; see Figure S2. For each ^{23}Na resonance, we extracted the underlying average quadrupolar product ($\overline{C}_{Q\eta} = \overline{C}_Q(1+\eta^2/3)^{1/2}$), isotropic chemical shift ($\overline{\delta}_{Na}^{iso}$) and its distribution width (W_{Na}^{iso}), by employing a program

DOI: 10.1021/acs.jpcb.5b01130
J. Phys. Chem. B 2015, 119, 5701−5715

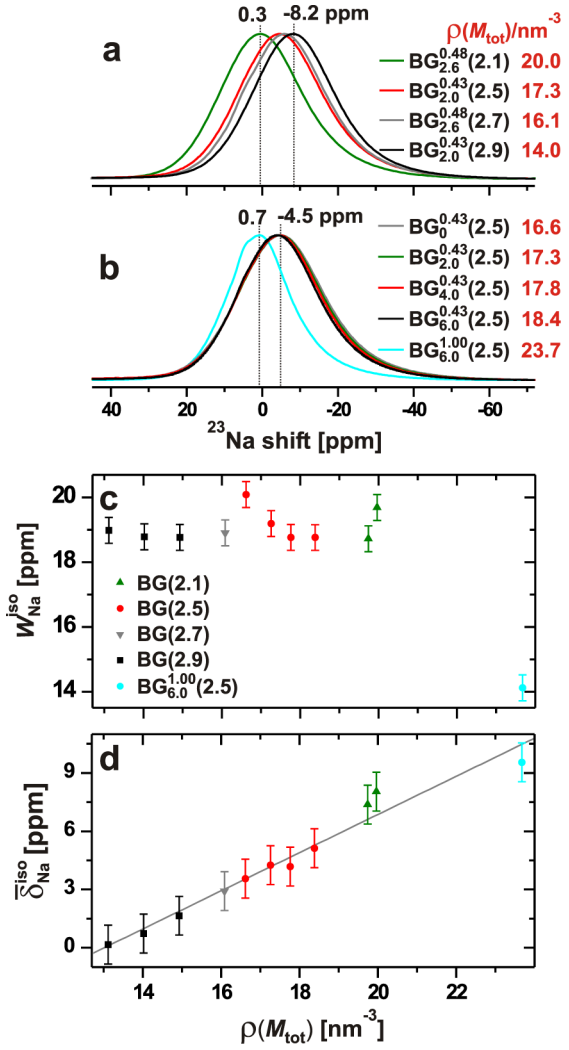

Figure 2. (a, b) ^{23}Na NMR spectra recorded at B_0 = 14.1 T and displayed for (a) increasing $\overline{N}^{Si}_{BO}$ (and thereby decreasing total modifier number density $\rho(M_{tot}) = \rho_{Na} + \rho_{Ca}$) at nearly constant P_2O_5 content of 2−3 mol %, and (b) for increasing amount of P_2O_5 at fixed $\overline{N}^{Si}_{BO}$ = 2.5. (c) Distribution width (W^{iso}_{Na}) of the ^{23}Na isotropic chemical shift plotted against $\rho(M_{tot})$. (d) ^{23}Na average isotropic chemical shift versus $\rho(M_{tot})$. Straight lines represent best-fit results.

developed in our laboratory.[50] The best-fit data and further details about the spectra deconvolutions are presented in Table S3. Note that all ^{23}Na parameters reported herein constitute average values over all coexisting Na coordinations (see section 5.2).

Throughout the series of mixed-Ca/Na BGs, a nearly constant value $\overline{C}_{Q\eta} \approx 3.6$ MHz is observed (in good agreement with that of $\overline{C}_{Q\eta}$ = 3.4 MHz previously reported from "45S5"[51]), while the ^{23}Na isotropic chemical-shift *distribution* width (W^{iso}_{Na}) varies marginally between 18.7−20.1 ppm (2.97−3.19 kHz at B_0 = 14.1 T); see Figure 2c and Table S3. The corresponding fwhm span of the ^{23}Na NMR peaks is 24.7−26.3 ppm; these values accord well with those of ref 15 that were obtained from SiO_2-rich (and P-free) soda-lime silicate glasses, where the invariance of the fwhm was attributed to a preference for mixed Na/Ca−SiO_4 contacts. Within each fixed-$\overline{N}^{Si}_{BO}$ branch, W^{iso}_{Na} decreases slightly for increasing P content of the glass (Figure 2c). Analogously with the ^{31}P nuclei of the Q^n_P species, the $BG^{1.00}_{6.0}(2.5)$ structure exhibits distinctly different ^{23}Na environments relative to those in any mixed Na−Ca−Si−P−O glass, reflected both in a significantly higher $\overline{\delta}^{iso}_{Na}$ value and a markedly narrower fwhm observed from $BG^{1.00}_{6.0}(2.5)$. The latter stems mainly from the reduced chemical-shift dispersion (W^{iso}_{Na} = 14.1 ppm) associated with more ordered ^{23}Na local environments around the Q^n_{Si} and Q^n_P groups in the Na_2O−SiO_2−P_2O_5 glass structure.

The BG series manifest altering ^{23}Na NMR peak positions, each being dictated by $\overline{\delta}^{iso}_{Na}$; the ^{23}Na average isotropic chemical shift depends foremost on the *total* network-modifier number density $\rho(M_{tot})$ in the structure, as evidenced both from the NMR spectra shown in Figure 2a and the data in panel d, which plots $\overline{\delta}^{iso}_{Na}$ against $\rho(M_{tot})$. This underscores that both Na^+/Ca^{2+} cations are in close spatial proximity, *together* balancing the negative charges of the various O species in the structure, as discussed previously in the context of (P-free) soda-lime silicate glasses.[15,52] The observed increase of $\overline{\delta}^{iso}_{Na}$ when $\rho(M_{tot})$ grows (accompanying a reduction in $\overline{N}^{Si}_{BO}$) may be rationalized from the relative partitioning of Na^+ around BO and NBO species,[52,53] where the BO population increases concurrently with $\overline{N}^{Si}_{BO}$. The herein established linear relationship between $\overline{\delta}^{iso}_{Na}$ and $\rho(M_{tot})$ in mixed-modifier silicate glasses is to our knowledge hitherto not reported, but is consistent with the shift-dependence on other structural factors proposed by Xue and Stebbins.[52] Only minute variations of the ^{23}Na NMR peak positions result when the P content of the BG is increased, simply reflecting that most of the Na^+ reservoir charge-balance the *dominating* glass network former, i.e., the SiO_4 moieties (also see section 5.5).

5.2. MD-Derived Na and Ca Coordinations. Na and Ca exhibit essentially identical *mean* coordination numbers $\overline{Z}_{Na-O}$ = 5.90 and $\overline{Z}_{Ca-O}$ = 5.92 (312 pm cutoff), as calculated over the *set* of 13 Na/Ca-bearing phosphosilicate glass models. The spread of (average) coordination numbers $\{Z_{Na-O}, Z_{Ca-O}\}$ among the *individual* glasses only manifest a weak composition-dependence, with the ranges 5.78−6.02 and 5.68−6.12 observed for Na and Ca, respectively, over all mixed-modifier glasses. These values are consistent with previous MD reports from related glass compositions.[20,25,37,53−56] Figure 3 reveals that 6-fold coordinations dominate each distribution of $\{NaO_p\}$ and $\{CaO_p\}$ polyhedra, with significant contributions from p = 5 and p = 7 coordinations. While the span of coordination numbers is somewhat larger for Ca compared with Na across the *glass series*, Ca manifests a slightly narrower distribution of coexisting coordination polyhedra $\{CaO_p\}$ within *each glass* structure, with the respective mean distribution widths $\overline{\sigma}_{Na}$ = 1.0 (total span $0.94 \leqslant \sigma_{Na} \leqslant 1.04$) and $\overline{\sigma}_{Ca}$ = 0.85 ($0.78 \leqslant \sigma_{Ca} \leqslant 0.90$) observed over all mixed-modifier Na−Ca−Si−(P)−O glass models. The feature $\sigma_{Ca} < \sigma_{Na}$ reflects the higher field-strength of the divalent Ca^{2+} ion relative to its monovalent Na^+ counterpart, thereby allowing Ca^{2+} to better control its own coordination environments.[16]

Introducing P to each soda-lime-silicate base composition $BG^{0.43}_0(2.5)$ or $BG^{0.43}_0(2.9)$ only provides a minor growth of both Z_{Na-O} and Z_{Ca-O} by $\lesssim$5% when the P_2O_5 content increases up to 6 mol % (at constant $\overline{N}^{Si}_{BO}$). Yet, despite the invariance of the $\{NaO_p\}$ and $\{CaO_p\}$ populations and their associated average coordination numbers Z_{Na-O} and Z_{Ca-O} in all *mixed*-modifier glass structures, the corresponding Na/Ca data differ markedly in each respective limiting Na and Ca based silicate glass of equal/comparable network connectivity: the two CaO−SiO_2 structures [$BG^0_0(2.0)$ and $BG^0_0(2.5)$] reveal relatively high Z_{Ca-O}-values of 6.44 and 6.29, respectively; see

DOI: 10.1021/acs.jpcb.5b01130
J. Phys. Chem. B 2015, 119, 5701−5715

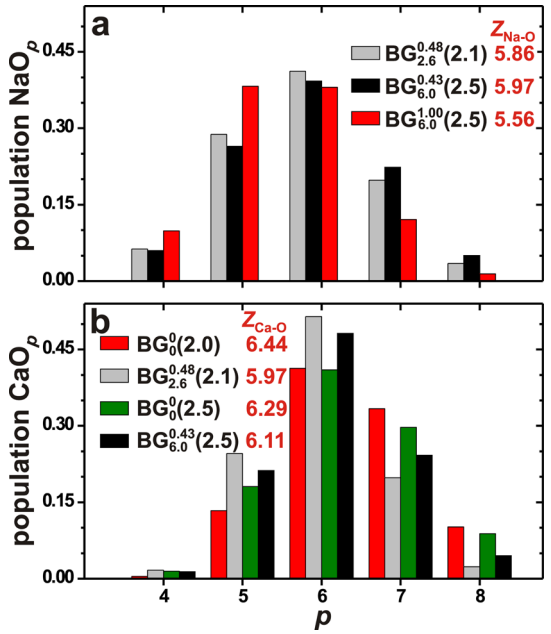

Figure 3. Fractional populations of (a) NaO_p and (b) CaO_p polyhedra plotted against the coordination number p for two $Na_2O-CaO-SiO_2-P_2O_5$ glasses, together with results from (a) the $Na_2O-SiO_2-P_2O_5$ glass $BG^{1.00}_{6.0}(2.5)$, as well as (b) two $CaO-SiO_2$ glasses, $BG^{0}_{0}(2.0)$ and $BG^{0}_{0}(2.5)$. The legends also specify the respective average coordination numbers Z_{Na-O} and Z_{Ca-O}.

Figure 3. The $Na_2O-SiO_2-P_2O_5$ glass $BG^{1.00}_{6.0}(2.5)$, on the other hand, exhibits a markedly lower average coordination number Z_{Na-O} = 5.56 relative to that of 5.97 in its $Na_2O-CaO-SiO_2-P_2O_5$ counterpart $BG^{0.43}_{6.0}(2.5)$. The feature $Z_{Na-O} \approx Z_{Ca-O}$ in the *mixed* glasses likely underlies the near-random Na/Ca partitioning around the various $\{Q^n_{Si}\}$ and $\{Q^n_P\}$ species discussed in section 5.5, because both network modifiers may readily replace each other around the network and only electrostatic Q^n_T-M restrictions control the substitutions.

Yet, a main distinction between Na^+ and Ca^{2+} is their propensities for coordination of BO/NBO species, where the globally emphasized Ca–NBO and Na–BO contacts (at the expense of Ca–BO and Na–NBO) are well documented.[16,20,25,55] Across the present glass series, Na–NBO accounts for 56–81% of all Na–O contacts, whereas the corresponding range for Ca–NBO is 83–91%. For both Na and Ca, the relative fraction of M–NBO bonds decreases when $\overline{N}^{Si}_{BO}$ is increased, whereas it grows concomitantly with the P content of the BG. The former correlation follows directly from the definition of $\overline{N}^{Si}_{BO}$ as the average number of BO per SiO_4 group, while the latter reflects that *both* Na and Ca coordinate the phosphate groups and their high number of NBO species.

5.3. Interatomic Na–P and Na–Si Contacts Probed by Heteronuclear NMR. *5.3.1. $^{23}Na \leftrightarrow ^{31}P$ NMR Results.* $^{23}Na\{^{31}P\}$ REDOR and $^{31}P\{^{23}Na\}$ REAPDOR NMR dephasing curves were recorded from a majority of the BG specimens. The extent of signal dephasing in S{I} REDOR/REAPDOR grows with the amount of I species in the structure. Figure 4a shows selected REDOR data recorded from glasses with increasing P_2O_5 content. The extent of dephasing indeed increases concurrently with ρ_P, reflecting a progressively growing number of phosphate groups around the Na^+ sites.

The second moment $M_2(Na-P)$ of each effective $^{23}Na-^{31}P$ dipolar contact was extracted by numerically fitting the experimental $\Delta S/S_0$ data associated with *short* $\tau_{rec} = 2n\tau_r$ values to eq 2. Figure 4c exemplifies zooms of the initial REDOR NMR dephasing regime, together with the best-fit results. The initial signal-dephasing rate increases when the

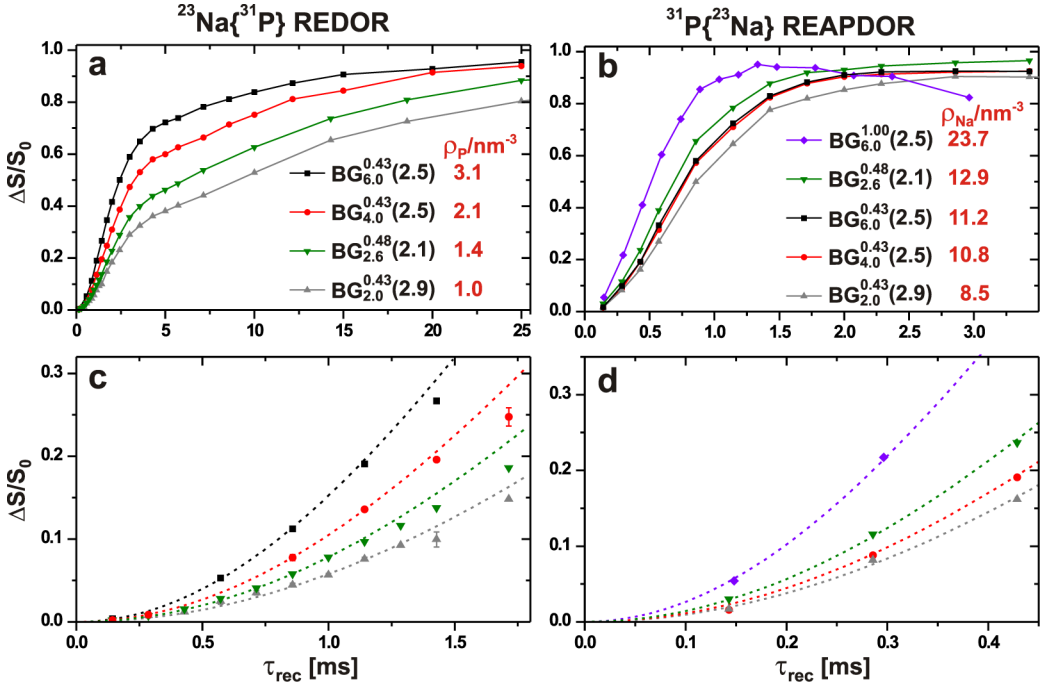

Figure 4. (a) $^{23}Na\{^{31}P\}$ REDOR and (b) $^{31}P\{^{23}Na\}$ REAPDOR NMR dephasing curves plotted against the recoupling period (τ_{rec}) for a selection of phosphosilicate glasses with increasing (a) ρ_P and (b) ρ_{Na}. (c, d) Zooms of the initial dephasing regimes in the respective plots (a, b), where the dashed lines represent best-fit results to eq 2 of the data $\Delta S/S_0 \leqslant 0.10$ (REDOR) and $\Delta S/S_0 \leqslant 0.20$ (REAPDOR). Error bars within the symbol sizes are not shown.

DOI: 10.1021/acs.jpcb.5b01130
J. Phys. Chem. B 2015, 119, 5701–5715

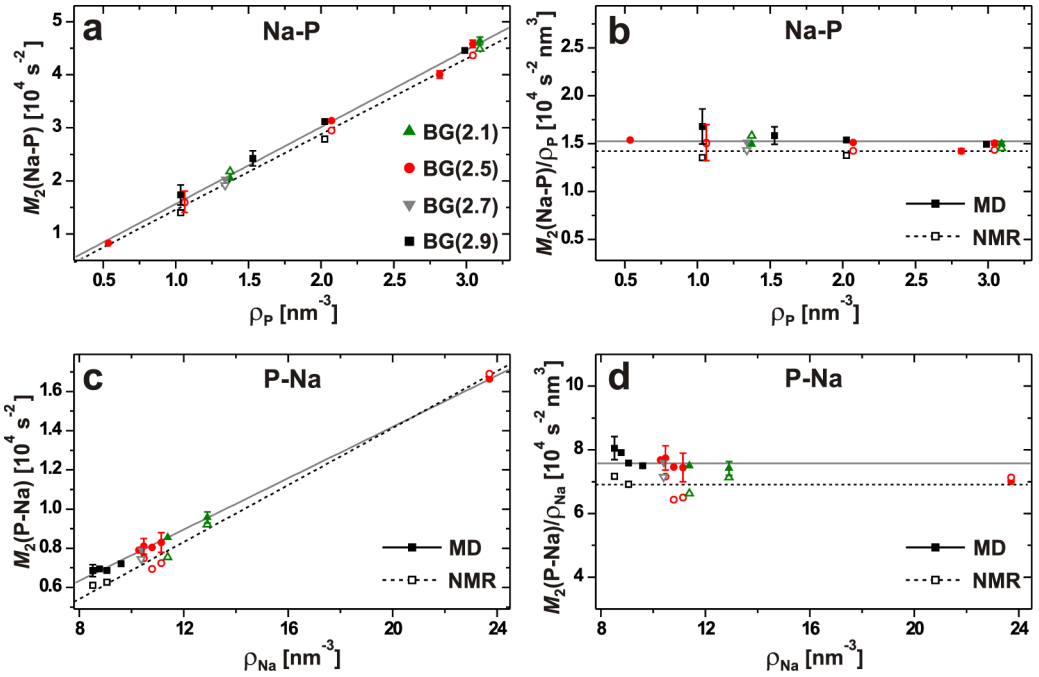

Figure 5. Dipolar second moments obtained either from MD simulations (solid symbols) or REDOR/REAPDOR NMR experiments (open symbols) and plotted against the number density of (a, b) P, or (c, d) Na, in the $Na_2O-CaO-SiO_2-P_2O_5$ glass. The right column plots normalized (b) $M_2(Na-P)/\rho_P$ data and (d) $M_2(P-Na)/\rho_{Na}$: note that the vertical plot-range for each of (b), (d) is selected to be directly comparable with the relative changes among the data in (a), (c), respectively. The solid and dashed lines in the left panel represent best-fit results of the MD and NMR data, respectively, whereas those of the right panels are positioned at the mean values of the second moments. Error bars below the symbol sizes are not shown.

P_2O_5 content of the BG grows. The set of estimated $M_2(Na-P)$-values is listed in Table S4, after (partial) correction for systematic errors primarily stemming from rf inhomogeneity; see the SI. Our data analysis is described in detail by Stevensson et al.[47] Dipolar second moments calculated from eq 1 and the atom coordinates of the MD-derived glass models are also presented. It is gratifying that the deviations between the experimental and modeled data generally stay below 5%, except for those of the BG(2.9) glass branch, which deviate up to 20%.

Figure 4(b, d) present selected $^{31}P\{^{23}Na\}$ REAPDOR NMR curves for glasses with increasing Na content. Similar trends to the REDOR case are observed, with the sole distinction that the signal dephasing is now dictated by ρ_{Na}. Figure 4d displays the initial $\Delta S/S_0$ regime versus τ_{rec}, with accompanying best-fit results to eq 2. The extracted $M_2(P-Na)$ values are given in Table S4, together with the corresponding MD-generated results.

Figure 5(a, c) plot the NMR/MD-derived second moments against ρ_P and ρ_{Na}, respectively, in both cases verifying linear trends and very good agreements between the experimental and modeled results, particularly for the $M_2(Na-P)$ data. The linear correlation between each ρ_P and ρ_{Na} number density and the respective $M_2(Na-P)$ and $M_2(P-Na)$ data sets suggests the absence of pronounced Na−P clustering tendencies in any $BG_p^q(\overline{N}_{BO}^{Si})$ glass structure. If there is a complete aggregation of species I around S, i.e., if fixed-n SI_n clusters form, then $M_2(S-I)$ remains essentially constant and independent of ρ_I, whereas if the I nuclei are randomly distributed in the structure, $M_2(S-I)$ grows linearly with ρ_I, such that the *ratio* $M_2(S-I)/\rho_I$ is constant.[2,12,14,57] Indeed, the $M_2(Na-P)/\rho_P$ and $M_2(P-Na)/\rho_{Na}$ results plotted in Figure 5(b, d) evidence very similar results among the glasses, with the scatter around the average values (horizontal lines) conveying the extents of deviations from a random distribution of Na^+ around the phosphate groups (and *vice versa*). These deviations are quantified further in section 5.7.

5.3.2. $^{23}Na\leftrightarrow^{29}Si$ NMR Results. As opposed to the 100% naturally abundant ^{23}Na and ^{31}P isotopes, the 4.7% abundance of ^{29}Si (the only NMR-active nuclide of Si) makes $^{29}Si\{^{23}Na\}$ double-resonance experimentation extremely time-consuming for attaining a reasonable signal sensitivity. Conversely, the dipolar recoupling dynamics of the "reverse" $^{23}Na\{^{29}Si\}$ NMR experiments becomes prohibitively slow as only 4.7% of all SiO_4 groups around the ^{23}Na sites contribute to the NMR signal dephasing. For these reasons, the Na−Si contacts in the BGs were assessed via MD simulations, except for two glass compositions that were prepared with 99.9% ^{29}Si enrichment. Figure 6a displays the $^{23}Na\{^{29}Si\}$ REDOR and $^{29}Si\{^{23}Na\}$ REAPDOR dephasing curves obtained from the $BG_{6.0}^{0.43}(2.5)$ and $BG_{6.0}^{1.00}(2.5)$ specimens, which only differ in their Ca and Na contents, where the latter glass is devoid of Ca. The initial REDOR/REAPDOR dephasing regimes are displayed in Figure 6b, together with the best-fit curves to eq 2 used to extract the $M_2(Na-Si)$ and $M_2(Si-Na)$ values. Table S4 lists the results and the corresponding MD-derived second moments. A good agreement is again observed between the experiments and MD models, except for the REAPDOR data of the Na−Si−P−O glass, as discussed in the SI.

The overall very good accordance between the NMR/MD-extracted second moments of the $^{23}Na-^{31}P$ and $^{23}Na-^{29}Si$ pairs is encouraging for pursuing analysis of the MD-derived glass models with confidence that they faithfully reflect the physical samples.

5.4. MD-Derived Relative Preferences for PO_4/SiO_4−Na/Ca Contacts. The coordination numbers $Z_{Na}^T \equiv Z(Q_T^n-Na)$ and $Z_{Ca}^T \equiv Z(Q_T^n-Ca)$ denote the average numbers of Na^+

DOI: 10.1021/acs.jpcb.5b01130
J. Phys. Chem. B 2015, 119, 5701−5715

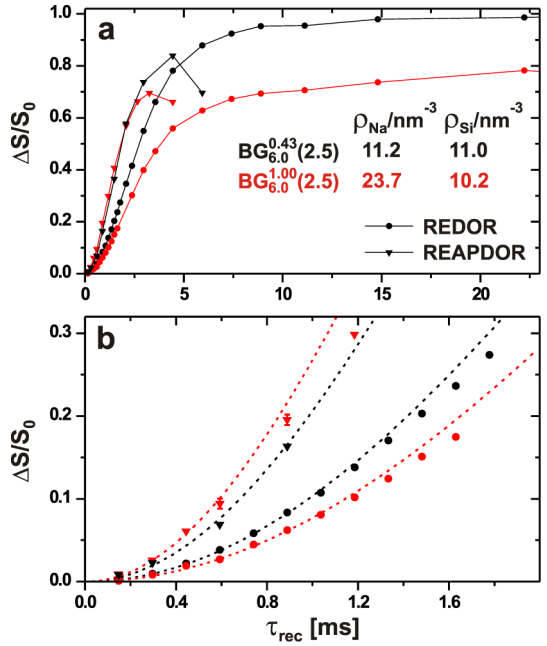

Figure 6. ^{23}Na{^{29}Si} REDOR (circles) and ^{29}Si{^{23}Na} REAPDOR (triangles) NMR dephasing curves recorded from the mixed-modifier $BG_{6.0}^{0.43}(2.5)$ glass and its Na–Si–P–O analogue $BG_{6.0}^{1.00}(2.5)$, displayed in black and red color, respectively. (b) Zoom of the initial dephasing regime, with dashed lines corresponding to best-fits to eq 2 of the experimental data obeying $\Delta S/S_0 \leqslant 0.10$ (REDOR) and $\Delta S/S_0 \leqslant 0.20$ (REAPDOR). Error bars below the symbol sizes are not shown.

and Ca^{2+} cations in the second coordination shell of the central T atom (Si or P) of the Q_T^n tetrahedron; we refer to them as the *first* coordination shell (FCS) of the Q_T^n *group* with respect to Na or Ca. The potential preferences for each tetrahedral $\{Q_P^n\}$ or $\{Q_{Si}^n\}$ species to coordinate either of Na or Ca may be evaluated from the ratio $R_{Na/Ca}(Q_T^n)$,[25,26]

$$R_{Na/Ca}(Q_T^n) = \frac{Z(Q_T^n\text{–Na})/x_{Na}}{Z(Q_T^n\text{–Ca})/x_{Ca}}, \quad T = \{P, Si\} \tag{3}$$

$R_{Na/Ca}(Q_T^n) = 1$ implies no preference for either modifier cation to associate around the given Q_T^n species, meaning that both Na^+ and Ca^{2+} are statistically distributed according to their respective relative molar fractions out of the total modifier reservoir:

$$x_M = \frac{n_M}{n_{Na} + n_{Ca}} = \frac{\rho_M}{\rho_{Na} + \rho_{Ca}}, \; M = \{Na, Ca\} \tag{4}$$

In contrast, whenever $R_{Na/Ca}(Q_T^n) > 1$ or $R_{Na/Ca}(Q_T^n) < 1$, the given Q_T^n species preferentially coordinates Na^+ and Ca^{2+} ions, respectively,[25,26,58] the precise meaning of which is clarified below.

The coordination numbers of eq 3 may either be evaluated over a suitable cutoff radius r (chosen as r = 450 pm in previous work[25,26,58]) or by requiring that each Si/P atom of the Q_T^n group shares O species with each modifier. Both sets of $R_{Na/Ca}(Q_T^n)$ values from the various Q_P^n and Q_{Si}^n groups are listed for each BG structure in Table S5. Except for the Q_{Si}^4–M contacts, they are very similar (as discussed further in the SI), and we onward base our analysis on the coordination numbers calculated from shared-oxygen T–O–M motifs.

Table S5 also includes the entities $R_{Na/Ca}(P)$ and $R_{Na/Ca}(Si)$ that constitute the aggregate factors representing the entire P and Si populations, respectively. Those two data sets reveal no striking differences if only considering their total ranges observed across the entire glass series, i.e., $0.87 \leqslant R_{Na/Ca}(P) \leqslant 0.95$ and $0.90 \leqslant R_{Na/Ca}(Si) \leqslant 1.05$. However, when comparing the propensities for cation coordinations among the individual $\{Q_{Si}^n, Q_P^n\}$ species and their dependencies on the BG composition, some distinct trends emerge: the preference for Na emphasizes—i.e., each $R_{Na/Ca}$-value increases—among the tetrahedral groups roughly according to

$$R_{Na/Ca}(Q_{Si}^1) < R_{Na/Ca}(Q_P^0) \approx R_{Na/Ca}(Q_{Si}^2) < R_{Na/Ca}(Q_P^1) \lesssim R_{Na/Ca}(Q_{Si}^3) \ll R_{Na/Ca}(Q_{Si}^4) \tag{5}$$

where the approximate relationship $R_{Na/Ca}(Q_P^n) \approx R_{Na/Ca}(Q_{Si}^{n+2})$ is noteworthy. These trends are clear from Figure 7 that plots

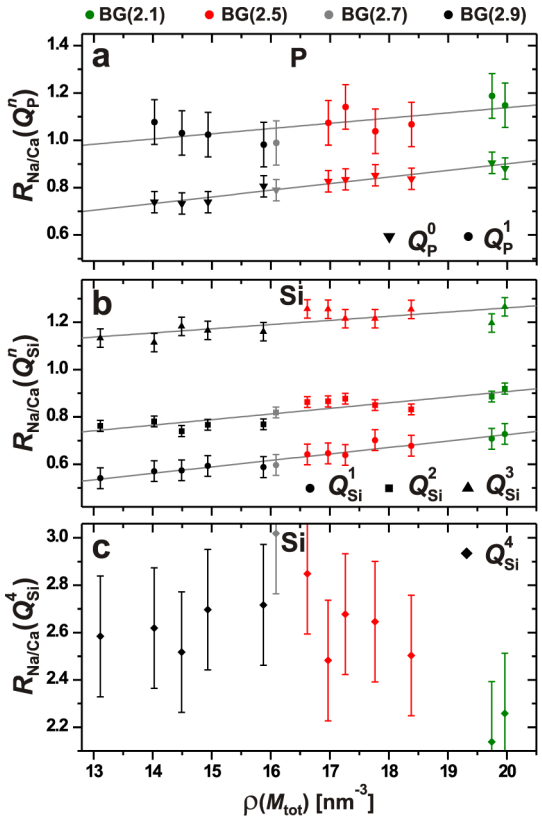

Figure 7. Plots of (a) $R_{Na/Ca}(Q_P^n)$ and (b, c) $R_{Na/Ca}(Q_{Si}^n)$ against $\rho(M_{tot})$. The distinct colors group samples $BG_p^q(N_{BO}^{Si})$ from each fixed-N_{BO}^{Si} branch, and the lines represent best-fit results. Note that all graphs employ the same vertical plot *ranges*. The cases $R_{Na/Ca}(Q_T^n) > 1$ and $R_{Na/Ca}(Q_T^n) < 1$ mark preference for the Q_T^n group to coordinate Na and Ca, respectively. The $R_{Na/Ca}$ factors were evaluated by requiring that the T and M species share O atoms.

$R_{Na/Ca}(Q_P^n)$ and $R_{Na/Ca}(Q_{Si}^n)$ against $\rho(M_{tot})$. The respective preferences for Q_{Si}^2–Ca and Q_{Si}^3–Na contacts accord with earlier inferences from ^{29}Si NMR on soda-lime-silicate-based glasses.[17,22] Note that data for the Q_{Si}^0 groups that exhibit the overall *strongest* associations with Ca^{2+} are not presented because their abundance is negligible in all our glass structures; see Table S1.[32]

Equation 5 underscores the importance of analyzing the relative Na/Ca preferences of each *individual* Q_T^n group, rather than attempting too generalized statements about the total "silicon" or "phosphorus" speciations[29,37,58,59] encoded by

DOI: 10.1021/acs.jpcb.5b01130
J. Phys. Chem. B 2015, 119, 5701–5715

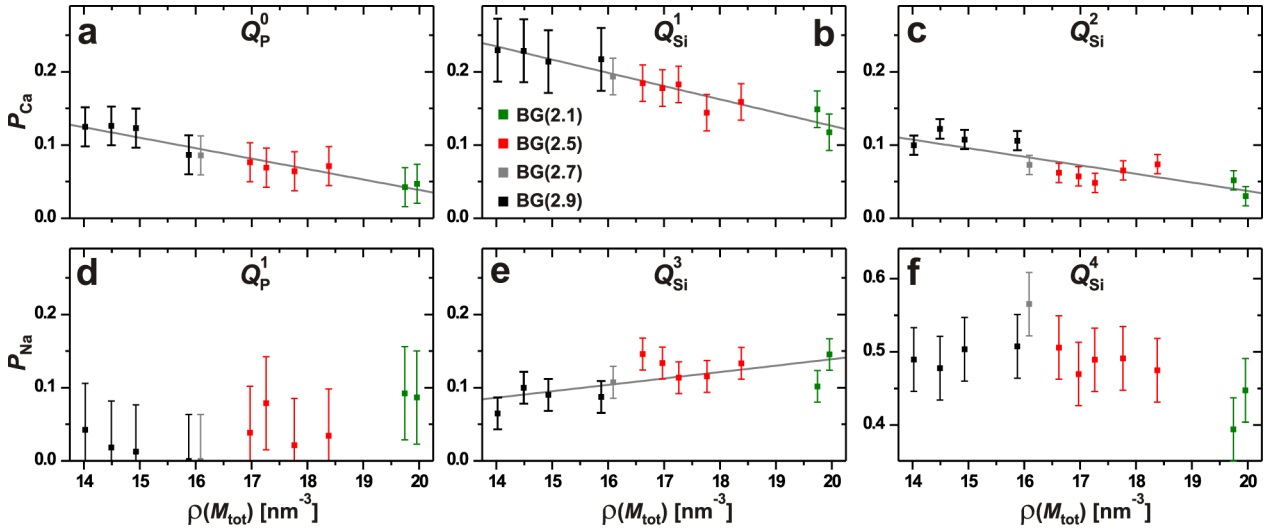

Figure 8. Plots of MD-derived preference factors (a–c) P_{Ca} and (d–f) P_{Na} against $\rho(M_{tot})$ for the as-indicated Q^n_T groups. The distinct colors group samples $BG^q_p(\overline{N}^{Si}_{BO})$ from each fixed-$\overline{N}^{Si}_{BO}$ branch and the lines represent best-fit results. Note that all plots employ the same vertical span of values [including (f)].

$R_{Na/Ca}(Si)$ and $R_{Na/Ca}(P)$, respectively. Notably, each of the latter constitutes a weighted average over the set $\{R_{Na/Ca}(Q^n_T)\}$ from the entire $\{Q^n_T\}$ ensemble, whose fractional populations $\{x^n_T\}$ *alter* when the glass composition varies (see Table S1). For instance, the $R_{Na/Ca}(Si)$-value from an arbitrary glass member within each distinct $\overline{N}^{Si}_{BO} = 2.1$ and $\overline{N}^{Si}_{BO} = 2.9$ branch is controlled by the Na/Ca partitioning around Q^2_{Si} and Q^3_{Si} species that *dominate* the SiO_4 speciation in the structure of each respective branch. To avoid overgeneralized statements about the "Si" or "P" species, we consistently discuss cation-coordination trends separately for each relevant Q^n_P ($n = 0, 1$) and Q^n_{Si} ($1 \leqslant n \leqslant 4$) moiety.

As previously pointed out,[25,26] simple electrostatic arguments readily explain the relative Na^+/Ca^{2+} partitioning among the various negatively charged silicate and phosphate moieties, where those bearing the highest charges—i.e., Q^0_P (PO^{3-}_4), Q^1_{Si} ($SiO^{3-}_{3.5}$), and Q^2_{Si} (SiO^{2-}_3)—experience significantly stronger attractions to the divalent Ca^{2+} cation compared with the monovalent Na^+ counterpart, whereas the latter naturally associate with the lower-charged groups, e.g., Q^3_{Si} ($SiO^{-}_{2.5}$). The trends of eq 5 may alternatively be rationalized from the variable numbers of BO/NBO species at each Q^n_T tetrahedron coupled with the pronounced propensities for Na–BO and Ca–NBO contacts (see section 5.2).

As discussed further in section 5.8, the Na/Ca intermixing around BO/NBO moieties in silicate glasses is accessible by ^{17}O NMR.[15,20] Such experiments *potentially* offer a route to estimate the factors $R_{Na/Ca}(BO) = x_{Ca}Z(BO–Na)/[x_{Na}Z(BO–Ca)]$ and $R_{Na/Ca}(NBO) = x_{Ca}Z(NBO–Na)/[x_{Na}Z(NBO–Ca)]$ that in analogy with eq 3 reveal the *net* tendency of each BO and NBO species to coordinate Na and Ca. However, there are two caveats: (*i*) Even application of high-resolution 3QMAS[60] ^{17}O NMR will not permit complete signal separation of the various Si–^{17}O–Si moieties associated with distinct modifier constellations involving either mixed Na/Ca species or solely each of Na or Ca.[20] Moreover, the 2D NMR spectra suffer from low signal sensitivity to detect minor ^{17}O species, such as P–^{17}O–Si moieties of Q^1_P groups (see the SI of ref 32 for discussions). (*ii*) While the factors $R_{Na/Ca}(BO)$ and $R_{Na/Ca}(NBO)$ are *related* to the set of $\{R_{Na/Ca}(Q^n_T)\}$ values, knowledge about the BO/NBO-based factors does not allow for *quantitatively* constructing the more informative set $\{R_{Na/Ca}(Q^n_T)\}$, even if each NBO, BO, $\{Q^n_P\}$, and $\{Q^n_{Si}\}$ fractional population is known. Hence, ^{17}O NMR and heteronuclear NMR experimentation provide closely related, yet distinct, *complementary* assessments of the Na/Ca intermixing in phosphosilicate glasses, probed from the viewpoints of the O and Si/P sites of the tetrahedral groups, respectively.

5.5. Quantifying the Na/Ca Ordering Around PO_4 and SiO_4 Groups. *5.5.1. The Procedure.* In general, *both* Na^+ and Ca^{2+} associate with each Q^n_T group, i.e., $Z^T_{tot} = Z(Q^n_T–Na) + Z(Q^n_T–Ca) = Z^T_{Na} + Z^T_{Ca}$. The relative Na/Ca abundances in the FCS of Q^n_T may represent any scenario between the following two limits: (*i*) A *complete preference* for *one* of the modifier species *M*, such that *M* occupies *all* positions out of the total coordination number Z^T_{tot} of the Q^n_T group with respect to all modifier species; for such a complete $Q^n_T–M$ aggregation/clustering, $Z(Q^n_T–M) = Z^T_{tot}$. (*ii*) A *statistical* distribution, where the numbers of *T*-associated Na^+ (Z^T_{Na}) and Ca^{2+} (Z^T_{Ca}) cations directly reflect their respective abundances, i.e., $Z^T_{Na} = x_{Na}Z^T_{tot}$ and $Z^T_{Ca} = x_{Ca}Z^T_{tot}$.

A random/statistical modifier partitioning is associated with $R_{Na/Ca}(Q^n_T) = 1$. Table S5 reveals that the most abundant building blocks of the BG structures, i.e., $\{Q^0_P, Q^1_P, Q^2_{Si}, Q^3_{Si}\}$, exhibit $R_{Na/Ca}(Q^n_T)$-values in the range 0.75–1.2, in agreement with earlier reports from a limited number of BG compositions.[25,26,58] However, while the $R_{Na/Ca}(Q^n_T)$ factor may *detect deviations* from the ideal statistical scenario, as well as identifying *which* Na^+/Ca^{2+} cation is preferred, it does *not convey* the *degree* of cation aggregation relative to the two limiting scenarios (*i*) and (*ii*).

We propose the following quantification of the *degree* of *preference*—$P_M(Q^n_T)$ [or P_M for short]—for a Q^n_T moiety to coordinate a cation species *M* (at the expense of another one, *M*′): P_M may assume values between $P_M = 0$ [statistical M/M' distribution; case (*ii*)] and $P_M = 1$ [all Z^T_{tot} positions are occupied by *M*; case (*i*)]. Any intermediate P_M-value encodes the relative contribution/weight of each statistical/full-aggregation scenario. The subscript "*M*" of P_M denotes the

DOI: 10.1021/acs.jpcb.5b01130
J. Phys. Chem. B 2015, 119, 5701–5715

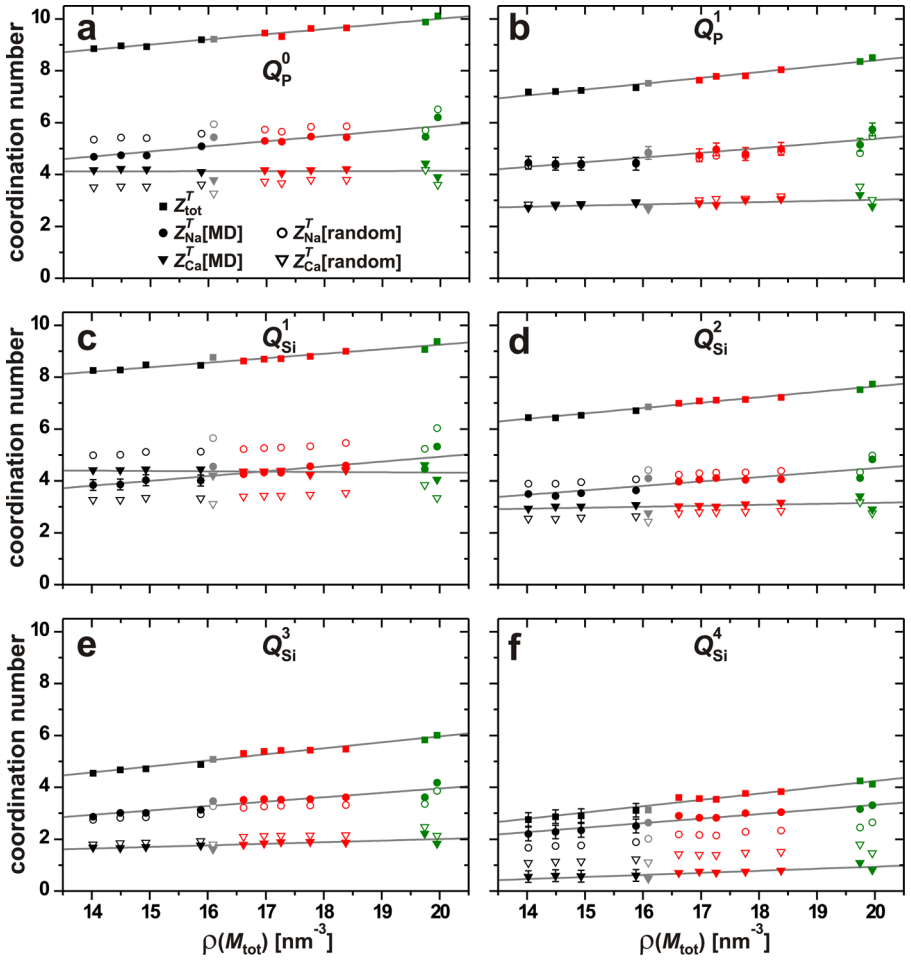

Figure 9. MD-derived total coordination number, $Z^T_{tot} = Z^T_{Na}+Z^T_{Ca}$, of the as-indicated Q^n_T group, plotted against $\rho(M_{tot})$ and shown together with each contribution from Na^+ (Z^T_{Na}) and Ca^{2+} (Z^T_{Ca}). The open symbols are values predicted from a statistical Na/Ca intermixing around each Q^n_T species. Straight lines represent best-fit results and demonstrate that all data depend nearly linearly on $\rho(M_{tot})$. The colors identify data from distinct N^{Si}_{BO}-branches, as in Figure 7.

preferred modifier species, which exhibits $R_{M/M'}(Q^n_T) > 1$. Note that $R_{M/M'}(Q^n_T) = [R_{M'/M}(Q^n_T)]^{-1}$ [see eq 3] and that the parameter *selected* out of the pair $\{P_M, P_{M'}\}$ is that whose *R*-factor is larger than unity. The preference factor P_M controls the average coordination numbers Z^T_M and $Z^T_{M'}$ of the Q^n_T group as follows:

$$Z^T_M = Z^T_{tot}[P_M + x_M(1 - P_M)] \quad (6)$$

$$Z^T_{M'} = Z^T_{tot}x_{M'}(1 - P_M) \quad (7)$$

The molar fractions x_M and $x_{M'}$ [eq 4] obey $x_M + x_{M'} = 1$. These expressions imply that *M* occupies $P_M Z^T_{tot}$ positions out of Z^T_{tot}, while the remaining $(1 - P_M)Z^T_{tot}$ positions are filled randomly with *both M* and *M′* according to their respective abundances in the structure. $P_M(Q^n_T)$ relates to $R_{M/M'}(Q^n_T)$ according to

$$R_{M/M'}(Q^n_T) = 1 + \frac{P_M(Q^n_T)}{x_M[1 - P_M(Q^n_T)]} \quad (8)$$

5.5.2. Trends among Q^n_T Groups in Phosphosilicate Glasses. The theoretical framework described above allows for directly assessing the propensity of a given Q^n_T group to coordinate Na^+ or Ca^{2+} cations by focusing on the FCS of the tetrahedron (i.e., the *second* coordination shell of Si or P). The results of P_{Ca} relevant for the Q^0_P, Q^1_{Si}, and Q^2_{Si} groups—as well as those for P_{Na} relevant for Q^1_P, Q^3_{Si}, and Q^4_{Si}—are readily calculated from eqs 6 and 7 by using the $\{Z^T_{Na}, Z^T_{Ca}, Z^T_{tot}\}$ values extracted from the MD-generated glass structures, only counting Na^+/Ca^{2+} ions *sharing* oxygen atoms with the central Si/P atom of the Q^n_T group. Figure 8 plots the results for each Q^n_T species. From the relationship eq 8 follows that the preference factors reveal the same trends as $R_{M/M'}(Q^n_T)$ of eq 5: for instance, $P_{Ca}(Q^0_P) \approx P_{Ca}(Q^2_{Si})$ and $P_{Na}(Q^1_P) \lesssim P_{Na}(Q^3_{Si})$. Yet, as opposed to $R_{M/M'}(Q^n_T)$, P_M conveys *directly* the relative contributions from the statistical scenario ($P_M = 0$) and the completely ordered case ($P_M = 1$) that together account for the modifier distribution around the Q^n_T moiety: disregarding the Q^4_{Si} groups that are markedly depleted of Ca^{2+} coordinations (see section 5.6), *all* Q^n_T species reveal *nearly statistical* Na/Ca distributions in their FCSs; the deviations typically remain within 15% ($P_M \lesssim 0.15$), except for the Q^1_{Si} groups ($0.12 \leqslant P_{Ca} \leqslant 0.25$).

Figure 9 plots the MD-derived coordination numbers $\{Z^T_{Na}, Z^T_{Ca}, Z^T_{tot}\}$ of each Q^n_T group against $\rho(M_{tot})$; it also includes the corresponding values predicted from a random Na/Ca partitioning to illustrate the consequences of the various P_M-values (Figure 8). Focusing on the set $\{Q^0_P, Q^1_P, Q^2_{Si}, Q^3_{Si}\}$ of most *abundant* structural moieties in BGs, none of the MD-modeled coordination numbers reveal any pronounced difference to those resulting from a statistical Na^+/Ca^{2+} intermixing.

DOI: 10.1021/acs.jpcb.5b01130
J. Phys. Chem. B 2015, 119, 5701−5715

For example, the value $P_{Ca}(Q^0_P)$ = 0.047 observed for the orthophosphate groups in the "45S5 Bioglass" [i.e., $BG^{0.48}_{2.6}(2.1)$] corresponds to MD-derived coordination numbers of Z^T_{Ca} = 3.91 and Z^T_{Na} = 6.21 that may be contrasted with Z^T_{Ca} = 3.60 and Z^T_{Na} = 6.51 predicted from a statistical distribution. These differences are insignificant. For the BG(2.9) glass-branch, whose Q^0_P groups exhibit the largest deviations from a statistical Na^+/Ca^{2+} intermixing ($P_{Ca}(Q^0_P)$ = 0.13; $R_{Na/Ca}(Q^0_P)$ = 0.73), the MD-modeled coordination numbers $\{Z^T_{Na}, Z^T_{Ca}\}$ = {4.74, 4.22} reveal non-negligible, but not striking, differences to those of the random distribution {5.42, 3.54}. This amounts to a 13% reduction of Z^T_{Na} accompanied by a 19% increase of Z^T_{Ca} in the simulated glasses.

We next consider the Q^1_{Si} groups in the modifier-poor BG(2.9) glasses that manifest the strongest deviations from a statistical Na/Ca partitioning, as mirrored in $P_{Ca}(Q^1_{Si}) \approx 0.23$ (Figure 8) and $R_{Na/Ca}(Q^1_{Si})$ = 0.57, i.e., $R_{Ca/Na}(Q^1_{Si})$ = 1.75 (see Table S5). The simulated values $\{Z^T_{Na}, Z^T_{Ca}\}$ = {3.59, 4.36} deviate more markedly from those of the random case $\{Z^T_{Na}, Z^T_{Ca}\}$ = {5.01, 3.27}, amounting to 28% lower (for Na) and 33% higher (for Ca) coordination numbers in the glass models. Worth stressing, however, is that the amounts of Q^1_{Si} moieties are negligible for all glass compositions where the deviations from the statistical scenario is most pronounced. For instance, in all $\overline{N}^{Si}_{BO} \geqslant 2.5$ glass branches that exhibit $P_{Ca}(Q^1_{Si})$>0.15, the *modeled* structures reveal $x^1_{Si} \approx 0.08$ [BG(2.5)] and $x^1_{Si} \approx 0.02$ [BG(2.9)], whereas the corresponding *experimental* fractions remain below 0.02 throughout (see Table S1).

5.6. Composition-Dependence of Si/P−Na/Ca Contacts. *5.6.1. Q^n_T−Na/Ca Preferences.* A reasonable coverage of the $Na_2O-CaO-SiO_2-P_2O_5$ glass system combined with independent variations of the two primary *in vitro* bioactivity arbitrators—i.e., the phosphate content (x_P) and the silicate network connectivity ($\overline{N}^{Si}_{BO}$)[32,42−45]—allows us to unveil the glass *composition*-dependence of the Na/Ca partitioning among the Q^n_{Si} and Q^n_P groups for the first time. We examined the correlation between each respective $\{R_{Na/Ca}(Q^n_T)\}$ and $\{P_M(Q^n_T)\}$ set and various conceivable glass composition parameters. Neither of the Si or P contents provides any transparent trend across the glass series. Both $R_{Na/Ca}(Q^n_T)$ and $P_M(Q^n_T)$ parameters depend on each of ρ_{Na} and ρ_{Ca} (and for the Q^2_{Si} and Q^3_{Si} groups, P_M also depends weakly on $\overline{N}^{Si}_{BO}$), but they correlate overall best with the total glass modifier number density, $\rho(M_{tot})$, against which roughly linear trends are observed: see Figures 7 and 8. When $\rho(M_{tot})$ is increased, weak but clearly discernible trends emerge: the relative preferences for Q^n_T−Na contacts generally *emphasize*, while those of Q^n_T−Ca *diminish*. The reduced preference of the most negatively charged TO_4 species to attract the divalent Ca^{2+} cations for increasing $\rho(M_{tot})$ likely stems from the globally increased positive charge-density in the glass structure, whereas the preference for Q^1_P−Na and Q^3_{Si}−Na contacts accentuate because additional monovalent cations are easier to accommodate than divalent ones of similar size.

The Si−**O**−Si bridges of the formally uncharged Q^4_{Si} tetrahedra manifest few close contacts with *any* modifier ion (Figure 9) and exhibit the most pronounced preference to associate with Na^+ rather than Ca^{2+} and its incompatibly high charge; see Figure 8. Both the $R_{Na/Ca}(Q^4_{Si})$ and $P_{Na}(Q^4_{Si})$ data display large uncertainties due to the small populations (Table S1), but the Q^4_{Si}−Na preference remains the only one that qualify as "strong" ($0.4 \lesssim P_{Na} \lesssim 0.55$).

5.6.2. Q^n_T−Na/Ca Coordination Numbers. We next consider the dependence of each (average) coordination number $Z_M(Q^n_T)$ on the phosphosilicate composition (see Figure 9). The Z^T_{Na} and Z^T_{Ca} values display a complex composition-dependence, with $\rho(M_{tot})$ providing the most transparent trend (out of several tested options): each coordination number increases concurrently with $\rho(M_{tot})$, where good linear correlations are observed for the Q^0_P and Q^1_P species. For all mixed-modifier glasses, the *total* coordination number is (*i*) generally larger for the $\{Q^n_P\}$ groups relative to those of $\{Q^n_{Si}\}$ and it (*ii*) grows together with the negative charge of the Q^n_T moiety according to

$$Q^4_{Si}(2.6-4.2) < Q^3_{Si}(4.4-6.0) < Q^2_{Si}(6.2-7.7) < Q^1_P(7.2-8.5) < Q^1_{Si}(7.9-9.4) < Q^0_P(8.9-10.1) \quad (9)$$

where the numbers within parentheses convey the spans observed across the set of BGs (see Figure 9). The composition-dependence of $Z_{tot}(Q^n_T)$ is discussed further in the SI that evidence excellent linear correlations for all Q^n_T groups either against $\rho(M_{tot})$ alone or versus the $\{\rho_P, \rho(M_{tot})\}$ parameter-pair.

A direct correlation between $Z_{Na}(Q^0_P)$ and ρ_{Na} [and also $\rho(M_{tot})$] readily explains the linear increase in the M_2(P−Na) data (Figure 5), as well as the monotonic ^{31}P chemical-shift trend of the Q^0_P groups observed both herein (Figure 1) and previously when ρ_{Na} [or $\rho(M_{tot})$] alters.[22−24,32,36,45] As follows from the combination of larger amounts of Na relative to Ca in our glasses and that the modifiers are almost statistically distributed, Z^T_{Na} is consistently larger than Z^T_{Ca} for each Q^n_T group (except for Q^1_{Si}; see Figure 9c). This feature implies that *despite* the minor *preference* for the Q^0_P and Q^1_P groups to coordinate Ca^{2+} and Na^+, respectively, the *net* Q^0_P−Na contacts are slightly *larger* than those of Q^1_P−Na because $Z_{Na}(Q^0_P) > Z_{Na}(Q^1_P)$. Indeed, comparable ^{31}P{^{23}Na} REAPDOR NMR-signal dephasing is observed from the Q^0_P and Q^1_P species (see Figure S4). Analogously, for the $BG^{1.00}_{6.0}(2.5)$ glass, Figure S5 confirms an expected faster ^{29}Si{^{23}Na} signal dephasing of the Q^2_{Si} groups relative to those of Q^3_{Si}, owing to $Z_{Na}(Q^2_{Si})>Z_{Na}(Q^3_{Si})$, *despite* the *preferences* for Q^2_{Si}−Ca and Q^3_{Si}−Na contacts, respectively.

5.7. Quantifying the P−Ca Preference by NMR. To ensure a transparent picture of the relative T−Na/Ca contacts, we considered solely the FCS of each Q^n_T group. Except for the Q^4_{Si} species, however, Z^T_{Na} and Z^T_{Ca} of a given Q^n_T moiety faithfully reflect the respective entities $M_2(Q^n_T-Na)$ and $M_2(Q^n_T-Ca)$ that rigorously account for the corresponding long-range (net) T−Na and T−Ca contacts in the structure, as discussed further in the SI. Consequently, the preference factor $P_M(Q^n_T)$ may be extracted from experimental $M_2(Q^n_T-M)$ data. For known number densities $\{\rho_{Na}, \rho_{Ca}\}$ of the phosphosilicate glass, the total coordination number $Z_{tot}(Q^n_T)$ is readily calculated (see the SI), which together with average $T-M$ distances estimated from our MD data for each Q^n_T group (Table S6) is used to determine $M_2(Q^n_T-Na)$ or $M_2(Q^n_T-Ca)$ for a $\{P_{Na}, P_{Ca}\}$ grid via eqs 1, 6 and 7. The preference is then deduced as the P_M-value whose associated $M_2(Q^n_T-M)$ result best matches its experimental counterpart. While the approach is generally applicable, it requires that $M_2(T-M)$ is experimentally accessible for each relevant Q^n_T group, which is in practice often problematic due to overlap of the NMR signals from distinct groups.

DOI: 10.1021/acs.jpcb.5b01130
J. Phys. Chem. B 2015, 119, 5701−5715

We applied the procedure to the NMR-derived M_2(P−Na) data presented in Figure 5c. Because orthophosphate moieties dominate the P speciation ($0.80 \lesssim x_P^0 \lesssim 0.96$; Table S1) and no significant differences were observed among the REAPDOR-signal dephasing from the Q_P^0 and Q_P^1 groups (Figure S4), we assumed that Q_P^0 alone contributes to the experimental M_2(P−Na) value of each Na−Ca−Si−P−O glass. Figure 10a displays

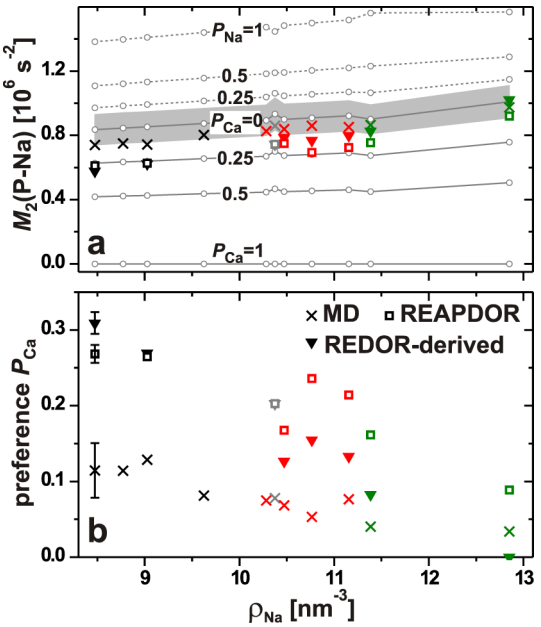

Figure 10. Experimental M_2(P−Na) results obtained from the mixed-modifier BG($\overline{N}_{BO}^{Si}$) glasses, either directly by ^{31}P{^{23}Na} REAPDOR NMR (open squares) or derived from the M_2(Na−P) values extracted by ^{23}Na{^{31}P} REDOR NMR (solid triangles).[47] Crosses represent MD-generated $M_2(Q_P^0$−Na) data. The open circles represent $M_2(Q_P^0$−Na) values calculated for different as-assumed preferences for the orthophosphate groups to coordinate Na (P_{Na}; dashed lines) or Ca (P_{Ca}; solid lines); they assumed total coordination numbers $Z_{tot}(Q_P^0)$ obtained from eq S1 and an average distance $\overline{r}_{P-Na}$ = 324 pm extracted from the MD-generated glass models; see Table S4. The gray area illustrates the effects of changing $Z_{tot}(Q_P^0)$ by ±1 in eqs 6 and 7, while $P_{Na} = P_{Ca} = 0$ is kept fixed. (b) Preference factors {P_{Ca}} extracted from the MD/NMR data in (a). The error-bars in (a) are within the symbols, whereas those in (b) are relatively uniform within each NMR/MD data set, as indicated for the first row of data, but omitted elsewhere for visualization purposes. The color coding is as in Figure 7.

M_2(P−Na) data determined either (*i*) *directly* from ^{31}P{^{23}Na} REAPDOR or (*ii*) *independently* from the {M_2(Na−P)} set obtained by ^{23}Na{^{31}P} REDOR NMR ("REDOR-derived"; see Table S4 and ref 47), as well as (*iii*) the MD-generated $M_2^{MD}(Q_P^0$−Na) results. Figure 10b plots the P_{Ca} value extracted from each method and glass. The NMR-derived {P_{Ca}} data are consistently 0.1−0.2 units higher than those of the glass models, with the largest differences resulting for the BG(2.9) branch. The preference factors span 0.09−0.27 (direct REAPDOR data), 0−0.31 (REDOR-derived), and {0.03−0.13} (MD) across all glasses.

A conservative uncertainty in the experimental *over*estimate of P_{Ca} is ≈ 0.1−0.2, if considering the multitude of experimental error sources, as well as the uncertainties of the MD data yielding the parameters {Z_{tot}^T, $\overline{r}_{T-M}$} input to the model; see the SI for further discussions. Nevertheless, the semiquantitative agreement between the three independent NMR/MD-deriving assessments firmly conclude that the Na/Ca intermixing around the Q_P^0 groups is nearly random, albeit some ordering effects are evident with preference for Q_P^0−Ca contacts that translate into a 10−30% excess of Ca^{2+} in the FCS compared with a statistical modifier distribution. The NMR results also corroborate the findings from the MD simulations that the Na/Ca intermixing tend to randomize when $\rho(M_{tot})$ is increased.

5.8. Cation Intermixing Around Oxygen Species in Soda-Lime-Silicate Glasses. As pointed out previously,[15,18] various studies targeting "cation intermixing" in glasses often lead to different conclusions. There may be several reasons for this: (**1**) concepts like "ordering" and "preference" depends on the precise choice of *reference*; (**2**) different *methods* are used for *probing* the ordering, as well as that (**3**) the *interpretation* of very similar data is up to subjective interpretations that may result in different conclusions. We assess the Na/Ca intermixing by comparing the relative preferences for Q_T^n−Na and Q_T^n−Ca coordinations. They only convey the relative $T-M$ contacts and neither provide information about the spatial *dispersion* of the network modifiers *across* the *structure*, nor about the relative Na−Na, Ca−Ca and Na−Ca associations. The latter are encoded by the PDFs $g_{Na-Na}(r)$, $g_{Ca-Ca}(r)$, and $g_{Na-Ca}(r)$, respectively, which do not inform directly about the relative preferences for the modifiers to coordinate the O sites around Si or P.

To illustrate how different "interpretations/conclusions" may arise for very similar structural scenarios, we consider the Na/Ca intermixing around the BO and NBO species in soda-lime-silicate glasses and contrast our MD-derived results from the $BG_0^{0.43}(2.5)$ and $BG_0^{0.43}(2.9)$ glasses with those obtained by ^{17}O NMR by Lee and Stebbins[15] for a $BG_0^{0.5}(3.33)$ composition (in our notation), and by Pedone et al.[19] for a MD-generated $BG_0^{0.5}(2.67)$ structure. Both reports concluded a nonrandom Na/Ca intermixing around the NBO species, interpreted as a "...strong tendency for the formation of dissimilar cation pairs...".[15,19] The experimental study involved additional glasses with variable n_{Na}/n_{Ca} ratios. The ^{17}O NMR-derived fractional population of Na−NBO out of the total O speciation was consistently lower than the prediction from a random Na/Ca partitioning: for the $BG_0^{0.5}(3.33)$ glass, two independent experimental estimates yielded 13% and 18% Na−NBO, whereas a random intermixing predicted 33% and 20%, depending on the assumed total NBO coordination number of either three or four, respectively.[15]

Table S7 compares the MD-derived results for the present $BG_0^{0.43}(2.5)$ and $BG_0^{0.43}(2.9)$ glasses with those of refs 15, 19. The table lists the fractional populations of the various X−Na, X−Ca and X−Na/Ca fragments that imply O species coordinating solely Na, Ca, and "mixed modifiers", respectively, with X = {BO, NBO}. When considering the slightly higher Ca content in the present $BG_P^q(\overline{N}_{BO}^{Si})$ glasses ($q = x(Na_2O) = 0.43$ relative to $x(Na_2O) = 0.50$[15,19]), the various fractional populations agree very well between different glasses and reports: the NBO environments exhibit consistently higher NBO−Ca and NBO−Na/Ca contacts (at the expense of NBO−Na) relative to the predictions from a statistical Na/Ca intermixing, whereas the trend is reversed for the BO populations. While commensurate with a preference for mixed-modifier NBO environments, we believe that the data could equally well—or even better—be interpreted as propensities for NBO−Ca and BO−Na contacts, particularly in view of the well-known preferences for NBO−Ca and BO−

DOI: 10.1021/acs.jpcb.5b01130
J. Phys. Chem. B 2015, 119, 5701−5715

Na associations in silicate glasses[16,20,25,55,56] (see section 5.2). Note that each MD-derived *average* coordination number $Z(\mathrm{NBO}-M_{\mathrm{tot}}) \approx 3$ and $Z(\mathrm{BO}-M_{\mathrm{tot}}) \approx 1$ stems from an ensemble of distinct coordination numbers across all BO/NBO sites in the structure (see Table S7). This is accounted for in the random Na/Ca distribution that is formed as a weighted average over several binomial distributions.[19] Noteworthy, these populations differ slightly to those obtained from a single binomial result with fixed $Z(\mathrm{NBO}-M_{\mathrm{tot}}) = 3$ or $Z(\mathrm{BO}-M_{\mathrm{tot}}) = 1$; notably, the precise $Z(X-M_{\mathrm{tot}})$ values are generally unknown and need to be assumed in the analysis of experimental ^{17}O NMR data.[9,13,15]

We also believe that our findings about the relative Si/P−Na/Ca preferences in BGs are consistent with those of Pedone et al.[20] who studied "45S5 Bioglass" by ^{17}O NMR coupled with MD simulations: while they concluded "non-random" modifier distributions in the various Si/P−BO−Na/Ca and Si/P−NBO−Na/Ca structural moieties, the deviations observed from a statistical distribution were minor and appear to be fully consistent with our inferred *weak* ordering effects (low P_M-values), particularly when considering the assumptions made in the analysis[20] and also accounting for the experimental uncertainties in the ^{17}O NMR data (that were not stated in ref 20). Noteworthy, our results further evidence that the weak Na/Ca ordering remains intact throughout a wide range of P-bearing soda-lime-silicate based glass compositions.

6. CONCLUDING REMARKS

We comprehensively probed the nature of the Na/Ca intermixing around silicate and phosphate groups in a large series of (bioactive) phosphosilicate glasses, where the primary bioactivity-controlling parameters—the phosphate content and the silicate network connectivity—were varied independently over wide ranges. The first coordination shells of both SiO_4 and PO_4 tetrahedra in the MD-derived glass models are well-mimicked by randomly distributed Na^+/Ca^{2+} cations, with the minor "degrees of ordering" amounting to $P_M \lesssim 0.15$, where $P_M = 1$ implies the sole presence of species M around the given Q^n_T unit. The most negatively charged Q^0_P, Q^1_{Si}, and Q^2_{Si} groups present in BGs with relatively low network-modifier contents manifest the strongest preferences for the divalent Ca^{2+} cations, but this trend becomes less pronounced when $\rho(M_{\mathrm{tot}})$ increases, such that the relative associations of $\{Q^0_P, Q^1_{Si}, Q^2_{Si}\}$ with Na^+ and Ca^{2+} ions tend toward a statistical distribution, whereas the preference for Na^+ around the lower-charged Q^1_P and Q^3_{Si} species become emphasized. Yet, the P_M-value of each Q^n_T group only varies weakly among glass compositions that provide a "high" [such as "45S5"[21], i.e., $BG^{0.48}_{2.6}(2.1)$] or "low" (all BG(2.9) members) bioactivity.

Heteronuclear dipolar second moments calculated from the MD-generated glass models accorded very well with the results of ^{23}Na{S} REDOR and S{^{23}Na} REAPDOR NMR, where S = {^{29}Si, ^{31}P}. We demonstrated that the preference factors may be extracted from NMR-derived second moments: this approach is generally applicable for analysis of any $M_2(\mathrm{S}-M)$ data of a well-defined structural group "S", provided that its dipolar dephasing is accessible by NMR. A good agreement was observed between the MD-generated $P_{\mathrm{Ca}}(Q^0_P)$ values and those obtained from $M_2(\mathrm{P}-\mathrm{Na})$ data extracted from ^{31}P{^{23}Na} REAPDOR NMR. The experimental estimates were somewhat larger (by ≈0.15) relative to the MD models, but the discrepancies are within the uncertainties from systematic errors inherent to this type of heteronuclear NMR experimentation.

For the same set of phosphosilicate glasses as considered herein, we previously concluded the absence of any pronounced phosphate clustering beyond that naturally associated with a (near) statistical dispersion.[31,33] This inference prevailed throughout the compositional space of all glass specimens. Hence, neither the spatial dispersion of PO_4 groups nor the relative preferences of the Q^n_T−Na/Ca contacts depend strongly on the silicate network connectivity or the P content. We conclude by reiterating our remark made in ref 33: the bioactivity-diminishing for BGs with $\overline{N}^{\mathrm{Si}}_{\mathrm{BO}} > 2.5$ most likely stems from the *globally inhibited* glass degradation associated with the highly polymerized silicate networks, rather than from significant cation aggregation/clustering effects at the (sub)nm scale. While the relationships between the network connectivity, the *in vitro* HCA formation rate, and the glass degradation ("solubility") are not strict, qualitative correlations emerge if also considering the field-strengths of the various network modifiers present in the phosphosilicate-based BGs, where glasses rich in high field-strength cations (e.g., Mg^{2+}, Ca^{2+}) degrade less than those incorporating lower field-strength ions (e.g., Na^+, K^+).[61,62] We propose that the glass bioactivity/solubility might be modeled *semiquantitatively* by using simple Si−O−Si and Si−O−M bond-strength considerations, because the Si−O−Si linkages and the number thereof at each Q^n_{Si} moiety dominate the energy landscape. Counts of the various bonds and extents of cross-linking within the silicate network might explain composition-solubility/bioactivity trends, thereby only invoking readily obtained *short-range* structural data (i.e., Q^n_{Si} populations), rather than seeking explanations in structural features over longer length-scales.

■ ASSOCIATED CONTENT

Supporting Information

Further information is provided about the following: details about the REDOR/REAPDOR NMR experimentation; tables of Q^n_{Si} and Q^n_P fractional populations, MD simulation parameters, R-factors conveying the relative Si/P↔Na/Ca contacts, best-fit ^{23}Na NMR parameters, NMR/MD-derived dipolar second moments, and BO−M and NBO−M contacts in soda-lime-silicate glasses; figures of rf-pulse diagrams, additional ^{23}Na MAS NMR spectra, ^{31}P{^{23}Na} and ^{29}Si{^{23}Na} REAPDOR NMR spectra; further information about the prediction of total coordination numbers of Na/Ca around each Q^n_T group; discussion about the limitations of heteronuclear dipolar-based and ^{17}O NMR experimentation for assessing relative Si/P↔Na/Ca and O↔Na/Ca contacts. This material is available free of charge via the Internet at http://pubs.acs.org.

■ AUTHOR INFORMATION

Corresponding Author

*E-mail: mattias.eden@mmk.su.se.

Notes

The authors declare no competing financial interest.

■ ACKNOWLEDGMENTS

This work was supported by the Swedish Research Council (contract 2010-4943) and the Faculty of Science at Stockholm University. We gratefully acknowledge NMR equipment Grants from the Swedish Research Council, and the Knut and Alice Wallenberg Foundation. We would like to thank an anonymous reviewer for insightful comments.

DOI: 10.1021/acs.jpcb.5b01130
J. Phys. Chem. B 2015, 119, 5701−5715

REFERENCES

(1) Zachariasen, W. H. The Atomic Arrangement in Glass. *J. Am. Chem. Soc.* **1932**, *54*, 3841−3851.
(2) Eckert, H.; Elbers, S.; Epping, J. D.; Janssen, M.; Kalwei, M.; Strojek, W.; Voigt, U. Dipolar Solid State NMR Approaches Towards Medium-Range Structure in Oxide Glasses. *Topics Curr. Chem.* **2005**, *246*, 195−233.
(3) Edén, M. NMR Studies on Oxide-Based Glasses. *Annu. Rep. Prog. Chem., Sect. C: Phys. Chem.* **2012**, *108*, 177−221.
(4) Day, D. E. Mixed Alkali Glasses - Their Properties and Uses. *J. Non-Cryst. Solids* **1976**, *21*, 343−372.
(5) Sato, R. K.; Kirkpatrick, R. J.; Brow, R. K. Structure of Li, Na Metaphosphate Glasses by ^{31}P and ^{23}Na MAS-NMR Correlated with the Mixed Alkali Effect. *J. Non-Cryst. Solids* **1992**, *143*, 257−264.
(6) Vessal, B.; Greaves, G. N.; Marten, P. T.; Chadwick, A. V.; Mole, R.; Houde-Walter, S. Cation Microsegregation and Ionic Mobility in Mixed Alkali Glasses. *Nature* **1992**, *356*, 504−506.
(7) Swenson, J.; Matic, A.; Karlsson, C.; Börjesson, L.; Meneghini, C.; Howells, W. S. Random Ion Distribution Model: A Structural Approach to the Mixed-Alkali Effect in Glasses. *Phys. Rev. B* **2001**, *63*, 1322021−1322024.
(8) Yap, A. T-W.; Förster, H.; Elliott, S. R. Spin-Echo Double Resonance NMR Evidence for Preferential Like-Cation Clustering in Mixed-Alkali Disilicate Glasses. *Phys. Rev. Lett.* **1995**, *75*, 3946−3949.
(9) Florian, P.; Vermillion, K. E.; Grandinetti, P. J.; Farnan, I.; Stebbins, J. F. Cation Distribution in Mixed Alkali Disilicate Glasses. *J. Am. Chem. Soc.* **1996**, *118*, 3493−3497.
(10) Gee, B.; Eckert, H. Cation Distribution in Mixed-Alkali Silicate Glasses. NMR Studies by ^{23}Na-{^{7}Li} and ^{23}Na-{^{6}Li} Spin Echo Double Resonance. *J. Phys. Chem.* **1996**, *100*, 3705−3712.
(11) Ratai, E.; Janssen, M.; Eckert, H. Spatial Distributions and Chemical Environments of Cations in Single- and Mixed Alkali Borate Glasses: Evidence from Solid State NMR. *Solid State Ionics* **1998**, *105*, 25−37.
(12) Ratai, E.; Chan, J. C. C.; Eckert, H. Local Coordination and Spatial Distribution of Cations in Mixed-Alkali Borate Glasses. *Phys. Chem. Chem. Phys.* **2002**, *4*, 3198−3208.
(13) Lee, S. K.; Mysen, B. O.; Cody, G. D. Chemical Order in Mixed-Cation Silicate Glasses and Melts. *Phys. Rev. B* **2003**, *68*, 2142061−2142067.
(14) Tsuchida, J.; Schneider, J.; Orlandi de Oliveira, A.; Rinke, M. T.; Eckert, H. Sodium Distribution in Mixed Alkali K-Na Metaphosphate Glasses. *Phys. Chem. Chem. Phys.* **2010**, *12*, 2879−2887.
(15) Lee, S. K.; Stebbins, J. F. Nature of Cation Mixing and Ordering in Na-Ca Silicate Glasses and Melts. *J. Phys. Chem. B* **2003**, *107*, 3141−3148.
(16) Cormack, A. N.; Du, J. Molecular Dynamics Simulations of Soda-Lime-Silicate Glasses. *J. Non-Cryst. Solids* **2001**, *293−295*, 283−289.
(17) Jones, A. R.; Winter, R.; Greaves, G. N.; Smith, I. H. MAS NMR Study of Soda-Lime-Silicate Glasses with Variable Degree of Polymerization. *J. Non-Cryst. Solids* **2001**, *293−295*, 87−92.
(18) Cormier, L.; Calas, G.; Beuneu, B. Structural Changes Between Soda-Lime Silicate Glass and Melt. *J. Non-Cryst. Solids* **2011**, *357*, 926−931.
(19) Pedone, A.; Gambuzzi, E.; Menziani, M. C. Unambiguous Description of the Oxygen Environment in Multicomponent Aluminosilicate Glasses from ^{17}O Solid State NMR Computational Spectroscopy. *J. Phys. Chem. C* **2012**, *116*, 14599−14609.
(20) Pedone, A.; Charpentier, T.; Malavasi, G.; Menziani, M. M. New Insights into the Atomic Structure of 45S5 Bioglass by Means of Solid-State NMR Spectroscopy and Accurate First-Principles Simulations. *Chem. Mater.* **2010**, *22*, 5644−5652.
(21) Hench, L. L. Bioceramics: From Concept to Clinic. *J. Am. Ceram. Soc.* **1991**, *74*, 1487−1510.
(22) Lockyer, M. W. G.; Holland, D.; Dupree, R. NMR Investigation of the Structure of Some Bioactive and Related Glasses. *J. Non-Cryst. Solids* **1995**, *188*, 207−219.
(23) Grussaute, H.; Montagne, L.; Palavit, G.; Bernard, J. L. Phosphate Speciation in Na_2O-CaO-P_2O_5-SiO_2 and Na_2O-TiO_2-P_2O_5-SiO_2 Glasses. *J. Non-Cryst. Solids* **2000**, *263*, 312−317.
(24) Elgayar, I.; Aliev, A. E.; Boccaccini, A. R.; Hill, R. G. Structural Analysis of Bioactive Glasses. *J. Non-Cryst. Solids* **2005**, *351*, 173−183.
(25) Tilocca, A.; Cormack, A. N.; de Leeuw, N. H. The Structure of Bioactive Silicate Glasses: New Insights from Molecular Dynamics Simulations. *Chem. Mater.* **2007**, *19*, 95−103.
(26) Tilocca, A.; Cormack, A. N. Structural Effects of Phosphorus Inclusion in Bioactive Silicate Glasses. *J. Phys. Chem. B* **2007**, *111*, 14256−14264.
(27) Leonova, E.; Izquierdo-Barba, I.; Arcos, D.; Lopez-Noriega, A.; Hedin, N.; Vallet-Regí, M.; Edén, M. Multinuclear Solid-State NMR Studies of Ordered Mesoporous Bioactive Glasses. *J. Phys. Chem. C* **2008**, *112*, 5552−5562.
(28) Gunawidjaja, P. N.; Lo, A. Y. H.; Izquierdo-Barba, I.; García, A.; Arcos, D.; Stevensson, B.; Grins, J.; Vallet-Regí, M.; Edén, M. Biomimetic Apatite Mineralization Mechanisms of Mesoporous Bioactive Glasses as Probed by Multinuclear ^{31}P, ^{29}Si, ^{23}Na and ^{13}C Solid State NMR. *J. Phys. Chem. C* **2010**, *114*, 19345−19356.
(29) Tilocca, A. Models of Structure, Dynamics and Reactivity of Bioglasses: A Review. *J. Mater. Chem.* **2010**, *20*, 6848−6858.
(30) Mercier, C.; Follet-Houttemane, C.; Pardini, A.; Revel, B. Influence of P_2O_5 Content on the Structure of SiO_2-Na_2O-CaO-P_2O_5 Bioglasses by ^{29}Si and ^{31}P MAS-NMR. *J. Non-Cryst. Solids* **2011**, *357*, 3901−3909.
(31) Mathew, R.; Turdean-Ionescu, C.; Stevensson, B.; Izquierdo-Barba, I.; García, A.; Arcos, D.; Vallet-Regí, M.; Edén, M. Direct Probing of the Phosphate-ion Distribution in Bioactive Silicate Glasses by Solid-State NMR: Evidence for Transitions Between Random/Clustered Scenarios. *Chem. Mater.* **2013**, *25*, 1877−1885.
(32) Mathew, R.; Stevensson, B.; Tilocca, A.; Edén, M. Toward a Rational Design of Bioactive Glasses with Optimal Structural Features: Composition-Structure Correlations Unveiled by Solid-State NMR and MD Simulations. *J. Phys. Chem. B* **2014**, *118*, 833−844.
(33) Stevensson, B.; Mathew, R.; Edén, M. Assessing the Phosphate Distribution in Bioactive Phosphosilicate Glasses by ^{31}P Solid-State NMR and MD Simulations. *J. Phys. Chem. B* **2014**, *118*, 8863−8876.
(34) FitzGerald, V.; Pickup, D. M.; Greenspan, D.; Sarkar, G.; Fitzgerald, J. J.; Wetherall, K. M.; Moss, R. M.; Jones, J. R.; Newport, R. J. A Neutron and X-ray Diffraction Study of Bioglass® with Reverse Mote-Carlo Modelling. *Adv. Funct. Mater.* **2007**, *17*, 3746−3753.
(35) Martin, R. A.; Twyman, H. L.; Rees, G. J.; Barney, E. R.; Moss, R. M.; Smith, J. M.; Hill, R. G.; Chibin, G.; Charpentier, T.; Smith, M. E.; et al. An Examination of the Calcium and Strontium Site Distribution in Bioactive Glasses Through Isomorphic Neutron Diffraction, X-ray Diffraction, EXAFS and Multinuclear Solid State NMR. *J. Mater. Chem.* **2012**, *41*, 2212−2223.
(36) O'Donnell, M. D.; Watts, S. J.; Law, R. V.; Hill, R. G. Effect of P_2O_5 Content in Two Series of Soda Lime Phosphosilicate Glasses on Structure and Properties-Part I: NMR. *J. Non-Cryst. Solids* **2008**, *354*, 3554−3560.
(37) Xiang, Y.; Du, J. Effect of Strontium Substitution on the Structure of 45S5 Bioglasses. *Chem. Mater.* **2011**, *23*, 2703−2717.
(38) Gullion, T.; Schaefer, J. Detection of Weak Heteronuclear Dipolar Coupling by Rotational-Echo Double-Resonance Nuclear Magnetic Resonance. *Adv. Magn. Reson.* **1989**, *13*, 57−83.
(39) Gullion, T. Measurement of Dipolar Interactions between Spin-1/2 and Quadrupolar Nuclei by Rotational-Echo, Adiabatic-Passage, Double-Resonance NMR. *Chem. Phys. Lett.* **1995**, *246*, 325−330.
(40) Bertmer, M.; Eckert, H. Dephasing of Spin Echoes by Multiple Heteronuclear Dipolar Interactions in Rotational Echo Double Resonance NMR Experiments. *Solid State Nucl. Magn. Reson.* **1999**, *15*, 139−152.
(41) Strojek, W.; Kalwei, M.; Eckert, H. Dipolar NMR Strategies for Multispin Systems Involving Quadrupolar Nuclei: ^{31}P{^{23}Na} Rotational Echo Double Resonance (REDOR) of Crystalline Sodium Phosphates and Phosphate Glasses. *J. Phys. Chem. B* **2004**, *108*, 7061−7073.

DOI: 10.1021/acs.jpcb.5b01130
J. Phys. Chem. B 2015, 119, 5701−5715

(42) Strnad, Z. Role of the Glass-Phase in Bioactive Glass-Ceramics. *Biomaterials* **1992**, *13*, 317−321.
(43) Hill, R. An Alternative View of the Degradation of Bioglass. *J. Mater. Sci. Lett.* **1996**, *15*, 1122−1125.
(44) Edén, M. The Split Network Analysis for Exploring Composition-Structure Correlations in Multi-Component Glasses: I. Rationalizing Bioactivity-Composition Trends of Bioglasses. *J. Non-Cryst. Solids* **2011**, *357*, 1595−1602.
(45) O'Donnell, M. D.; Watts, S. J.; Hill, R. G.; Law, R. V. The Effect of Phosphate Content on the Bioactivity of Soda-Lime Phosphosilicate Glasses. *J. Mater. Sci: Mater. Med.* **2009**, *20*, 1611−1618.
(46) Van Vleck, J. H. The Dipolar Broadening of Magnetic Resonance Lines in Crystals. *Phys. Rev. Lett.* **1948**, *74*, 1168−1183.
(47) Stevensson, B.; Mathew, R.; Yu, Y.; Edén, M. Two Hetero nuclear Dipolar Results at the Price of One: Quantifying Na/P Contacts in Phosphosilicate Glasses and Biomimetic Hydroxy-Apatite. *J. Magn. Reson.* **2015**, *251*, 52−56.
(48) Smith, W.; Forester, T. R. DL_POLY_2.0: A General-Purpose Parallel Molecular Dynamics Simulation Package. *J. Mol. Graphics* **1996**, *14*, 136−141.
(49) Todorov, I. T.; Smith, W.; Trachenko, K.; Dove, M. T. DL_POLY_3: New Dimensions in Molecular Dynamics Simulations via Massive Parallelism. *J. Mater. Chem.* **2006**, *16*, 1911−1918.
(50) Pahari, B.; Iftekhar, S.; Jaworski, A.; Okhotnikov, K.; Jansson, K.; Stevensson, B.; Grins, J.; Edén, M. Composition-Property-Structure Correlations of Scandium Aluminosilicate Glasses Revealed by Multinuclear ^{45}Sc, ^{27}Al and ^{29}Si Solid State NMR. *J. Am. Ceram. Soc.* **2012**, *95*, 2545−2553.
(51) Pedone, A.; Charpentier, T.; Menziani, M. C. The Structure of Fluoride-Containing Bioactive Glasses: New Insights from First-Principles Calculations and Solid State NMR Spectroscopy. *J. Mater. Chem.* **2012**, *22*, 12599−12608.
(52) Xue, X.; Stebbins, J. F. ^{23}Na NMR Chemical Shifts and Local Na Coordination Environments in Silicate Crystals, Melts and Glasses. *Phys. Chem. Miner.* **1993**, *20*, 297−307.
(53) Charpentier, T.; Ispas, S.; Profeta, M.; Mauri, F.; Pickard, C. First-Principles Calculation of ^{17}O, ^{29}Si and ^{23}Na NMR Spectra of Sodium Silicate Crystals and Glasses. *J. Phys. Chem. B* **2004**, *108*, 4147−4161.
(54) Mead, R. N.; Mountjoy, G. A Molecular Dynamics Study of the Atomic Structure of $(CaO)_x(SiO_2)_{1-x}$ Glasses. *J. Phys. Chem. B* **2006**, *110*, 14273−14278.
(55) Tilocca, A.; de Leeuw, N. H. Structural and Electronic Properties of Modified Sodium and Soda-Lime Silicate Glasses by Car-Parrinello Molecular Dynamics. *J. Mater. Chem.* **2006**, *16*, 1950−1955.
(56) Pedone, A.; Malavasi, G.; Menziani, M. Computational Insight into the Effect of CaO/MgO Substitution on the Structural Properties of Phospho-Silicate Bioactive Glasses. *J. Phys. Chem. C* **2009**, *113*, 15723−15730.
(57) Voigt, U.; Lammert, H.; Eckert, H.; Heuer, A. Cation Clustering in Lithium Silicate Glasses: Quantitative Description by Solid-State NMR and Molecular Dynamics Simulations. *Phys. Rev. B* **2005**, *72*, 064207.
(58) Tilocca, A. Cooling Rate and Size Effects on the Medium-Range Structure of Multicomponent Oxide Glasses Simulated by Molecular Dynamics. *J. Chem. Phys.* **2013**, *139*, 114501.
(59) Malavasi, G.; Pedone, A.; Menziani, M. C. Study of the Structural Role of Gallium and Aluminum in 45S5 Bioactive Glasses by Molecular Dynamics Simulations. *J. Phys. Chem. B* **2013**, *117*, 4142−4150.
(60) Frydman, L.; Harwood, J. S. Isotropic Spectra of Half-Integer Quadrupolar Spins from Bidimensional Magic-Angle-Spinning NMR. *J. Am. Chem. Soc.* **1995**, *117*, 5367−5368.
(61) Rawlings, R. D. Composition Dependence of the Bioactivity of Glasses. *J. Mater. Sci. Lett.* **1992**, *11*, 1340−1343.
(62) Martin, R. A.; Twyman, H. L.; Rees, G. J.; Smith, J. M.; Barney, E. R.; Smith, M. E.; Hanna, J. V.; Newport, R. J. A Structural Investigation of the Alkali Metal Site Distribution within Bioactive Glass Using Neutron Diffraction and Multinuclear Solid State NMR. *Phys. Chem. Chem. Phys.* **2012**, *14*, 12105−12113.

DOI: 10.1021/acs.jpcb.5b01130
J. Phys. Chem. B 2015, 119, 5701−5715